Advances in Space Research, Volume 67, Issue 3, February 2021, pp. 1174-1187
DOI:10.1016/j.asr.2020.10.047

Backstepping sliding-mode control of stratospheric airships using disturbance-observer

Shi Qian Liu[a,b *], James F. Whidborne[b], Lei He[c, b]

[a] *School of Aeronautics and Astronautics, Shanghai Jiao Tong University, Shanghai 200240, China*

[b] *School of Aerospace, Transport and Manufacturing, Cranfield University, Cranfield MK43 0AL, UK*

[c] *School of Aerospace, College of Aeronautics, Northwestern Polytechnical University, Xi'an, China*

Abstract In the presence of unknown disturbances and model parameter uncertainties, this paper develop a nonlinear backstepping sliding-mode controller (BSMC) for trajectory tracking control of a stratospheric airship using a disturbance-observer (DO). Compared with the conventional sliding mode surface (SMS) constructed by a linear combination of the errors, the new SMS manifold is selected as the last back-step error to improve independence of the adjustment of the controller gains. Furthermore, a nonlinear disturbance-observer is designed to process unknown disturbance inputs and improve the BSMC performances. The closed-loop system of trajectory tracking control plant is proved to be globally asymptotically stable by using Lyapunov theory. By comparing with traditional backstepping control and SMC design, the results obtained demonstrate the capacity of the airship to execute a realistic trajectory tracking mission, even in the presence of unknown disturbances, and aerodynamic coefficient uncertainties.

Keywords: stratospheric airship system; sliding mode control; nonlinear disturbance observer; backstepping control; trajectory tracking

1. Introduction

The stratospheric airship has been receiving a growing interest from both industry and academia due to their potential cost including high altitude, long endurance UAVs with vertical take-off and landing, low

* Correspondence to: Shiqian Liu, School of Aeronautics and Astronautics, Shanghai Jiao Tong University, Shanghai, P. R. China, 200240
Academic visitor, Center for Aeronautics, Cranfield University, UK, MK43 0AL
† E-mail address: liushiqian@sjtu.edu.cn (S.Q. Liu), j.f.whidborne@cranfield.ac.uk (J.F. Whidborne), heleidsn@mail.nwpu.edu.cn (L. He)

power, and hovering advantages. They have growing applications in earth observation, climatological monitoring, environmental surveillance and communication relay. The core feature of the airship is autonomous capability during the mission.

The trajectory tracking is one of fundamental functions of the airship control system, but it is an uneasy task. The highly nonlinear dynamics together with unpredictable complex environment, which make model uncertainties such as varying apparent mass and inertia of the airship, and the authority of control surfaces reduced by low airspeeds (Azinheira et al., 2006). There are many studies on trajectory tracking problem of the airship in the literatures. Gain scheduling and PID are often preferred because they are easy realized (Moutinho and Azinheira, 2006; Valle, et al., 2015). However, linear control design approaches are hard to accomplish when nonlinear of the airship motion is emphasized under environment disturbances and low airspeed flight. Therefore nonlinear control methods are often applied to trajectory tracking control of the airship (Moutinho and Azinheira, 2004). To apply some 'good' nonlinearities, the Lyapunov based backstepping approach is proposed , the attractive qualities of backstepping are the asymptotic global stability against parametric uncertainty, whether matched or mismatched, and the systematic recursive construction of the Lyapunov functions (Slotine and Li, 1991). Azinheira et al.(2006, 2009) proposed backstepping control designs for hover stabilization and path-tracking of a nonlinear underactuated airship model. Liesk et al. (2013) proposed a waypoint tracking controller for an unmanned finless airship. Liu and Sang (2018) developed a vectorial backstepping method with active set control allocation to deal with saturation. However, these methods depend on the accurate model and are hard to deal with highly nonlinear airship dynamics with aerodynamic model uncertainties.

The other mainstream nonlinear method of trajectory tracking control is sliding mode control (SMC). SMC is widely used due to its attractive features like insensitivity to matched uncertainties, robustness to external perturbations, simplicity and ease of implementation, and finite-time convergence (Edwards and Spurgeon, 1998; Yang and Yan, 2016; Zheng and Sun, 2018; Lou et al, 2019; Chen and Edwards, 2020).

Yang and Yan (2016) proposed a neural network approximation-based sliding-mode approach for positioning control of an autonomous airship. After that, Yang (2018) proposed nonsingular terminal sliding mode control for trajectory tracking control of a robotic airship. In order to take advantage of the benefits of both SMC and backstepping control approaches, Bolivar et al. (1997) combined them and developed a backstepping sliding mode controller (BSMC1). Another type, BSMC2 has been developed whose SMS manifold is selected as the last back step error to improve independence of the adjustment of the controller gains (Bolivar and Zinober, 1994). Adhikary and Mahanta (2013) proposed an integral backstepping sliding mode control for the cart–pendulum system. For the airship control, Chen (2017) proposed a BSMC for three-degree-of-freedom trajectory tracking of the stratospheric airship. Parsa et al.(2018) presented an integral BSMC for station keeping of the stratospheric airship. Vieira (2019) compared three methods of BS, SMC, BSMC and applied them to control a NOAMAY airship. To improve system adaptiveness, Liu et al. (2020) proposed an adaptive sliding-mode-backstepping trajectory tracking control for underactuated airships.

Since airships working in the stratosphere often meet unknown disturbances such as winds, coupling effects from other subsystems, and environmental and sun radiation noise, a nonlinear disturbance observer-based control (DOBC) approach is introduced in this paper to enhance the disturbance attenuation ability and performance robustness of the BSMC. The disturbance observer-based technique has been applied to the control of nonlinear systems and systems with unknown disturbances for decades (Chen et al., 2016), where an observer is designed to estimate external disturbances or ignore nonlinear dynamics and then compensate for them (Hu et al., 2018). Chen (2003) proposed a composite controller based on DO for the autopilot of a missile. Guo and Chen (2005) proposed a DOBC for disturbance attenuation and rejection for systems with nonlinearity. Li et al. (2014) gave detailed design methods of DOBC and applied them to control a hypersonic vehicle.

Motivated by the work of Verira (2019) and Chen (2003), this paper mainly concerns trajectory tracking

control for the stratospheric airship, and the main contributions are listed as follows: a novel disturbance-observer based backstepping sliding-mode control (DO-BSMC) is proposed for a stratospheric airship. A new SMS manifold is selected as the last back-step error to achieve additional degree of freedom. The composite controller of the DO-BSMC consists of a BSMC and a nonlinear disturbance observer, thus effect of large unknown disturbance inputs and model parameter uncertainties can be effectively reduced. The DO-BSM composite controller has a two-level control structure including a trajectory guider and an attitude and velocity controller, and its properties such as stability are established. Simulation results show the proposed DO-BSMC control has better performances in the trajectory tracking control for a stratospheric airship compared with BSMC methods.

This paper is organized as follows. Section 2 gives the nonlinear dynamics model of the stratospheric airship and presents the trajectory tracking problem. Section 3 proposes the DO-BSMC control design, and stability is analyzed for the associated closed-loop tracking system. Simulations and performances of two scenarios with the DO-BSMC control are demonstrated in Section4. The final section gives some conclusions.

2. Dynamics modeling and problem formulation

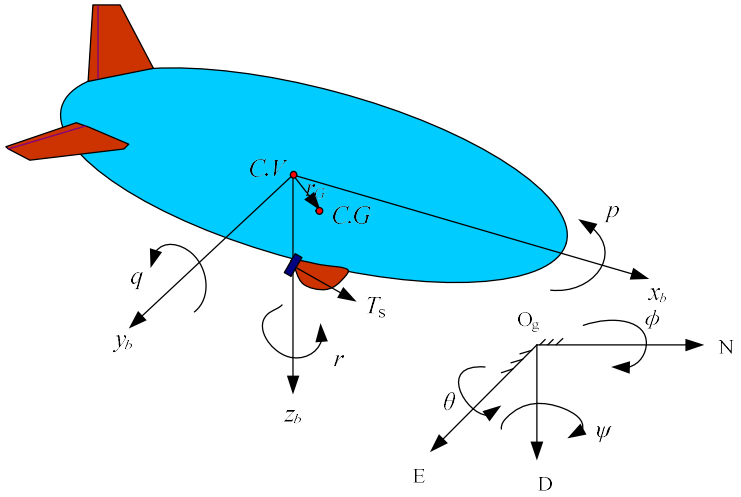

Fig. 1. Structure of the stratospheric airship

The considered model is a 250m length, 75m diameter airship (Mueller et al., 2004), the structure

parameters and aerodynamic coefficients of the stratospheric airship are listed in Table 1.

Table 1 Parameters and coefficients for the studied airship

Parameter	Value	Coefficient	Value
m	5.3×10^4 (kg)	k_1	0.1054
ρ	0.072 (kg/m^3)	k_2	0.8259
vol	7.4×10^5 (m^3)	k_3	0.1247
L	250 (m)	C_z	− 657
x_G, z_G	0, 20 (m)	C_l	2.4×10^4
d_x, d_z	5, 5 (m)	C_m	-7.7×10^4
I_x	4×10^7(kg·m^2)	C_n	-7.7×10^4
I_y	2.3×10^8(kg·m^2)	δ_e	(−25, 25) (°)
I_z	2.2×10^8(kg·m^2)	δ_e	(−25, 25) (°)
I_{xz}	-4.8×10^6(kg·m^2)	T_x, T_z	3×10^6 (N)

2.1 Airship Kinematics Model

The studied stratospheric airship is shown in Fig.1. The kinematics model of the airship's position and attitude is given by (Moutinho et al. 2016; Liu and Sang, 2018):

$$\dot{\boldsymbol{x}}_1(t) = \boldsymbol{T}\boldsymbol{x}_2(t) \tag{1}$$

where $\boldsymbol{x}_1 = \begin{bmatrix}\boldsymbol{\xi}^T & \boldsymbol{\eta}^T\end{bmatrix}^T$, $\boldsymbol{x}_2 = \begin{bmatrix}\boldsymbol{\upsilon}_a^T & \boldsymbol{\omega}^T\end{bmatrix}^T$, $\boldsymbol{\xi} = \begin{bmatrix}x & y & z\end{bmatrix}^T$ represents the airship position in the inertial frame, $\boldsymbol{\eta} = \begin{bmatrix}\phi & \theta & \psi\end{bmatrix}^T$ is the attitude vector, $\boldsymbol{\upsilon}_a = \begin{bmatrix}u & v & w\end{bmatrix}^T$ and $\boldsymbol{\omega} = \begin{bmatrix}p & q & r\end{bmatrix}^T$ are the speed and angular rate in the body frame respectively, and

$$\boldsymbol{T} = \begin{bmatrix}\boldsymbol{R}(\boldsymbol{\eta}) & \boldsymbol{0} \\ \boldsymbol{0} & \boldsymbol{J}(\boldsymbol{\eta})\end{bmatrix} \tag{2}$$

where the direction cosine matrix $\boldsymbol{R}$ is

$$\boldsymbol{R}(\boldsymbol{\eta}) = \begin{pmatrix} c(\theta)c(\psi) & -c(\phi)s(\psi)+s(\phi)s(\theta)c(\psi) & s(\psi)s(\phi)+c(\phi)s(\theta)c(\psi) \\ c(\theta)s(\psi) & c(\phi)c(\psi)+s(\phi)s(\theta)s(\psi) & -s(\phi)c\psi+c(\phi)s(\theta)s(\psi) \\ -s(\theta) & s(\phi)c(\theta) & c(\theta)c(\phi) \end{pmatrix} \tag{3}$$

and the transformation matrix $\boldsymbol{J}$ is

$$\boldsymbol{J}(\boldsymbol{\eta})=\begin{pmatrix}1 & s(\phi)\tan\theta & c(\phi)\tan\theta\\ 0 & c(\phi) & -s(\phi)\\ 0 & s(\phi)\sec\theta & c(\phi)\sec\theta\end{pmatrix} \tag{4}$$

where $|\theta| < \pi/2$ is assumed to avoid the singularity of matrix because $\theta = \pm\pi/2$ is not likely to be encountered during practical operation of the airship, $s(.)$ and $c(.)$ denote sine and cosine functions respectively.

2.2 Airship Dynamics Model

The airship dynamics is represented by (Gomes, 1990; Moutinho et al., 2016; Liu et al., 2020):

$$\boldsymbol{M}_a\begin{bmatrix}\dot{\boldsymbol{\upsilon}}_a(t)\\ \dot{\boldsymbol{\omega}}(t)\end{bmatrix}=\begin{bmatrix}\boldsymbol{f}_k+\boldsymbol{f}_w+\boldsymbol{f}_{GB}+\boldsymbol{f}_A\\ \boldsymbol{n}_k+\boldsymbol{n}_w+\boldsymbol{n}_{GB}+\boldsymbol{n}_A\end{bmatrix}+\begin{bmatrix}\boldsymbol{f}_{CP}\\ \boldsymbol{n}_{CP}\end{bmatrix}\quad, \tag{5}$$

where $\boldsymbol{M}_a$ denotes the generalized mass matrix as in Liu and Sang (2018). $\boldsymbol{f}_k$ denotes the kinetics force vector, $\boldsymbol{f}_w$ denotes the wind-induced force vector, $\boldsymbol{f}_{GB}$ denotes sum of the gravity and buoyancy vector, $\boldsymbol{f}_A$ denotes the aerodynamic force vector, $\boldsymbol{f}_{CP}$ denotes the control input and thrust vector, $\boldsymbol{n}_k$, $\boldsymbol{n}_w$, $\boldsymbol{n}_{GB}$, $\boldsymbol{n}_A$,and $\boldsymbol{n}_{CP}$ are associated moments generated by $\boldsymbol{f}_k$ $\boldsymbol{f}_w$, $\boldsymbol{f}_{GB}$, $\boldsymbol{f}_A$ and $\boldsymbol{f}_{CP}$,respectively. Let $U=\begin{bmatrix}\boldsymbol{f}_{CP}\\ \boldsymbol{n}_{CP}\end{bmatrix}$, then (5) can be rewritten as

$$\dot{\boldsymbol{x}}_2(t)=\boldsymbol{f}_2+\boldsymbol{g}_2U(t)\,, \tag{6}$$

where

$$\boldsymbol{f}_2=\boldsymbol{M}_a^{-1}.\begin{bmatrix}\boldsymbol{f}_k+\boldsymbol{f}_w+\boldsymbol{f}_{GB}+\boldsymbol{f}_A\\ \boldsymbol{n}_k+\boldsymbol{n}_w+\boldsymbol{n}_{GB}+\boldsymbol{n}_A\end{bmatrix}=\begin{bmatrix}(\boldsymbol{f}_{2V})_{3\times1}\\ (\boldsymbol{f}_{2\omega})_{3\times1}\end{bmatrix}, \tag{7}$$

$$\boldsymbol{g}_2(\boldsymbol{x})=\boldsymbol{M}_a^{-1}=\begin{bmatrix}(\boldsymbol{g}_{2V})_{3\times3} & (\boldsymbol{g}_{2V\omega})_{3\times3}\\ (\boldsymbol{g}_{2\omega V})_{3\times3} & (\boldsymbol{g}_{2\omega})_{3\times3}\end{bmatrix}. \tag{8}$$

$\boldsymbol{g}_{2V}$, $\boldsymbol{g}_{2V\omega}$, $\boldsymbol{g}_{2\omega V}$ and $\boldsymbol{g}_{2\omega}$ denote the sub-matrices of $\boldsymbol{M}_a^{-1}$. Airship aerodynamic force, kinetics force, sum force of gravity and buoyancy, and their moments on the right hand side of (5) are as in Gomes (1990), and Liu and Sang (2018). The thrust on the stern is not considered in flight, which is mainly used for hovering. For simplicity, two tilt angles and thrusts of the vectored propellers are assumed to be equal, and the effect

of rudders on the side force is also ignored. The virtual control force in (5) is described as

$$\boldsymbol{U}(t)=\begin{bmatrix}\boldsymbol{f}_{CP}\\ \boldsymbol{n}_{CP}\end{bmatrix}=\boldsymbol{B}\boldsymbol{u}(t)\ , \tag{9}$$

where $\boldsymbol{B}$ is the control effectiveness matrix, $\boldsymbol{u}$ represents thrusts and control surface deflections. If the airship is underactuated in the y-direction, or lacks lateral force effector to oppose aerodynamic side forces (Azinheira et al., 2006), then (9) can be rewritten as follows

$$\begin{bmatrix}f_{CPx}\\ f_{CPz}\\ n_{CPx}\\ n_{CPy}\\ n_{CPz}\end{bmatrix}=\begin{bmatrix}1 & 0 & 0 & 0 & 0 & 0\\ 0 & 1 & \bar{q}C_{z\delta_e} & \bar{q}C_{z\delta_e} & 0 & 0\\ 0 & 0 & \bar{q}C_{l\delta_e} & -\bar{q}C_{l\delta_e} & \bar{q}C_{l\delta_r} & -\bar{q}C_{l\delta_r}\\ dz & dx & \bar{q}C_{m\delta_e} & \bar{q}C_{m\delta_e} & 0 & 0\\ 0 & 0 & 0 & 0 & \bar{q}C_{n\delta_r} & \bar{q}C_{n\delta_r}\end{bmatrix}\begin{bmatrix}T_x\\ T_z\\ \delta_{eL}\\ \delta_{eR}\\ \delta_{rU}\\ \delta_{rB}\end{bmatrix}, \tag{10}$$

where $C_{z\delta_e},C_{l\delta_e},C_{l\delta_r},C_{m\delta_e},C_{n\delta_r}$ are aerodynamic coefficients of the control surfaces, T_x and T_z are thrust components in x_b axis and z_b axis, respectively. d_x and d_z denote distances from the CV to the propeller in the x_b- and z_b- axis. The thrusts in (10) can be linearized by the following transformation:

$$\begin{cases}T_x=\left(T_p+T_s\right)\cos\mu\\ T_z=-\left(T_p+T_s\right)\sin\mu\end{cases} \tag{11}$$

where T_p and T_s denote thrusts of the port side and starboard side respectively. And then the tilting angle can be obtained by μ=atan$(-T_z/T_x)$, the maximum and minimum values of the tilting angle are 90°and −90°.

Since there exist winds, environmental and sun-radiation noise for the stratospheric airship, then the model disturbance $\boldsymbol{f}$ is introduced and the system of (6) is modified to

$$\dot{\boldsymbol{x}}_2(t)=\boldsymbol{f}_2(\boldsymbol{x})+\boldsymbol{g}_2(\boldsymbol{x})U(t)+\boldsymbol{g}_3(\boldsymbol{x})\boldsymbol{f}(t) \tag{12}$$

where $\boldsymbol{f}\in\mathbb{R}^6$ denote model uncertainties and external disturbances, and it is assumed that $\boldsymbol{f}$ is bounded with $|\boldsymbol{f}|<f_\mathrm{U}, f_\mathrm{U}$ is a real value, $\boldsymbol{g}_3(x)=diag(\begin{bmatrix}1 & 1 & 1 & 1 & 1 & 1\end{bmatrix})$.

2.3 The Trajectory Tracking Control Problem

Consider the airship models of (1) and (12). Let $\xi_r(t):[0,\infty)\to\mathbb{R}^3$ be a given sufficiently smooth

time-varying reference trajectory with its time-derivatives ($\dot{\boldsymbol{\xi}}_r(t)$, $\ddot{\boldsymbol{\xi}}_r(t)$) bounded. The control task is to design a trajectory tracking controller such that the closed-loop system is globally asymptotically stable and the output trajectory $\boldsymbol{\xi}$ is steered towards a given reference trajectory $\boldsymbol{\xi}_r$ with $\lim_{t\to\infty}\|\boldsymbol{e}(t)\|_2 < \varepsilon_0$, even in specified model uncertainty and external disturbance environment, where tracking error $\boldsymbol{e}(t) = \boldsymbol{\xi}(t) - \boldsymbol{\xi}_r(t)$, ε_0 is a prescribed constant, 2-norm $\|\boldsymbol{e}(t)\|_2 = \sqrt{\boldsymbol{e}^T\boldsymbol{e}}$.

3 DO-BSMC trajectory tracking control design

This section gives an overview of the DO-BSMC control for the airship. The structure of the DO-BSMC control design includes a backstepping sliding mode based attitude controller, a nonlinear disturbance observer, a CLF based velocity controller, a virtual control calculation part and an active set control allocation module. The controller design is presented in detail in the next section.

3.1 Nonlinear Disturbance Observer Design

Since the tracking system of (12) has the unknown bounded disturbance $\boldsymbol{f}$, to improve the tracking precision, a nonlinear disturbance observer (NDO) is designed as follows (Chen et al., 2016),

$$\begin{cases} \dot{\hat{\boldsymbol{w}}}(t) = -\boldsymbol{l}(\boldsymbol{x})\boldsymbol{g}_3(\boldsymbol{x})\hat{\boldsymbol{w}}(t) - \boldsymbol{l}(\boldsymbol{x})\left(\boldsymbol{g}_3(\boldsymbol{x})\boldsymbol{p}(\boldsymbol{x}) + \boldsymbol{f}_2(\boldsymbol{x}) + \boldsymbol{g}_2(\boldsymbol{x})\boldsymbol{U}\right) \\ \hat{\boldsymbol{f}}(t) = \hat{\boldsymbol{w}}(t) + \boldsymbol{p}(\boldsymbol{x}) \end{cases} \tag{13}$$

where $\hat{\boldsymbol{w}} \in \mathbb{R}^q$ is the internal state of the nonlinear observer, and $\boldsymbol{p}(x)$ is the nonlinear function to be designed.

The NDO gain $l(x)$ is determined by

$$\boldsymbol{l}(x) = \frac{\partial \boldsymbol{p}(\boldsymbol{x})}{\partial \boldsymbol{x}} \tag{14}$$

It has been shown in Chen et al. (2016) that the NDO of Eq.(13) asymptotically estimates the disturbance if the observer gain $\boldsymbol{l}(\boldsymbol{x})$ is chosen such that Eq.(15) is global exponentially stable for all $\boldsymbol{x} \in \mathbb{R}^n$,

$$\dot{\boldsymbol{d}}(t) = \dot{\boldsymbol{f}}(t) - \dot{\hat{\boldsymbol{f}}}(t) = -\dot{\hat{\boldsymbol{f}}}(t) = -\dot{\hat{\boldsymbol{w}}}(t) - \frac{d\boldsymbol{p}(x)}{dt}$$

$$= \boldsymbol{l}(\boldsymbol{x})\boldsymbol{g}_3(\boldsymbol{x})\hat{\boldsymbol{w}}(t) + \boldsymbol{l}(\boldsymbol{x})\left(\boldsymbol{g}_3(\boldsymbol{x})\boldsymbol{p}(\boldsymbol{x}) + \boldsymbol{f}_2(\boldsymbol{x}) + \boldsymbol{g}_2(\boldsymbol{x})\boldsymbol{U}(t)\right) - \frac{d\boldsymbol{p}(\boldsymbol{x})}{dt}$$

$$= \boldsymbol{l}(\boldsymbol{x})\hat{\boldsymbol{f}}(t) - \boldsymbol{l}(\boldsymbol{x})\boldsymbol{f}(t)$$

$$= -\boldsymbol{l}(\boldsymbol{x})\boldsymbol{g}_3(\boldsymbol{x})\boldsymbol{d}(t) \tag{15}$$

where $\boldsymbol{d}$ denotes the unobservable part of the overall disturbance $\boldsymbol{f}$. The observable disturbances is usually can be measured and estimated by the observer, such as 1-cosine winds. The unobservable disturbance cannot be measured and hard to be observed by the observer, such as white noises. It has been shown that the estimation $\hat{\boldsymbol{f}}(t)$ of the NDO approaches the disturbance $\boldsymbol{f}(t)$ exponentially if the error dynamics of Eq.(15) is global exponentially stable (Chen et al., 2016).

Hence the disturbance compensator can be designed as

$$\boldsymbol{u}_f(t) = -\boldsymbol{g}_2^{-1}(\boldsymbol{x})\left(\boldsymbol{g}_3(\boldsymbol{x})\hat{\boldsymbol{f}}(t)\right) \tag{16}$$

Remark 1 The design of a disturbance observer (13) essentially is to choose an appropriate gain $\boldsymbol{l}(\boldsymbol{x})$ and associated $\boldsymbol{p}(\boldsymbol{x})$ such that the convergence of estimation error $\boldsymbol{d}(t)$ is guaranteed. It is possible to choose $\boldsymbol{l}(\boldsymbol{x})$ as a constant matrix such that all the eigenvalues of matrix $-\boldsymbol{l}(\boldsymbol{x})\mathbf{g}_3$ have negative real part. Integrating $\boldsymbol{l}(\boldsymbol{x})$ with respect to the airship state $\boldsymbol{x}$ yields $\boldsymbol{p}(\boldsymbol{x}) = \boldsymbol{l}\,\boldsymbol{x}$.

By using the proposed disturbance compensator (16), the effect of disturbances acting on the airship has been reduced. Therefore, a composite controller combined a backstepping SMC controller with the disturbance compensator is proposed as $\boldsymbol{U}(t)=\boldsymbol{U}_{BSMC}(t)+\boldsymbol{u}_f(t)$. By using Eqs (16), then the system (12) can be transformed as follows,

$$\dot{\boldsymbol{x}}_2(t) = \boldsymbol{f}_2(\boldsymbol{x}) + \boldsymbol{g}_2(\boldsymbol{x})\boldsymbol{U}(t) + \boldsymbol{g}_3(\boldsymbol{x})\boldsymbol{f}(t)$$

$$= \boldsymbol{f}_2(x) + \boldsymbol{g}_2(\boldsymbol{x})\left(\boldsymbol{U}_{BSMC}(t)+\boldsymbol{u}_f(t)\right) + \boldsymbol{g}_3(\boldsymbol{x})\boldsymbol{f}(t)$$

$$= \boldsymbol{f}_2(\boldsymbol{x}) + \boldsymbol{g}_2(\boldsymbol{x})\boldsymbol{U}_{BSMC}(t) - \boldsymbol{g}_2(\boldsymbol{x})\boldsymbol{g}_2^{-1}(x)\left(\boldsymbol{g}_3(\boldsymbol{x})\hat{\boldsymbol{f}}(t)\right) + \boldsymbol{g}_3(\boldsymbol{x})\boldsymbol{d}(t)$$

$$= \boldsymbol{f}_2(\boldsymbol{x}) + \boldsymbol{g}_2(\boldsymbol{x})\boldsymbol{U}_{BSMC}(t) + \boldsymbol{g}_3(\boldsymbol{x})\left(\boldsymbol{f}(t) - \hat{\boldsymbol{f}}(t)\right)$$

$$= \boldsymbol{f}_2(\boldsymbol{x}) + \boldsymbol{g}_2(\boldsymbol{x})\boldsymbol{U}_{BSMC}(t) + \boldsymbol{g}_3(\boldsymbol{x})\boldsymbol{d}(t) \tag{17}$$

3.2 Backstepping Sliding-mode Control Based Attitude Controller

This section is to design the backstepping sliding mode controller, and the objective is to make the attitude output $\boldsymbol{\eta}$ converge to the desired value vector $\boldsymbol{\eta}_d$. Now consider the kinematics model (1) and the dynamics model (17). The attitude controller is derived in two steps.

Step 1 (Backstepping for the variant of z_1).

The tracking error vector of attitudes is defined as

$$z_1 \triangleq \boldsymbol{\eta} - \boldsymbol{\eta}_d \,, \tag{18}$$

and its derivative is

$$\dot{z}_1 \triangleq \dot{\boldsymbol{\eta}} - \dot{\boldsymbol{\eta}}_d = J\boldsymbol{\omega} - \dot{\boldsymbol{\eta}}_d \quad . \tag{19}$$

Since the desired behavior for $\dot{\boldsymbol{\eta}}$ can still be chosen, it can be considered as the "virtual" control input. In the backstepping design this desired dynamic behavior is called the stabilizing function. Define the stabilizing function α, as the virtual angular rate vector of $\dot{\boldsymbol{\eta}}_r$

$$\alpha \triangleq \dot{\boldsymbol{\eta}}_d - K_1 z_1 \,, \tag{20}$$

where $\dot{\boldsymbol{\eta}}_r$ represents the reference or virtual angular rate vector, $K_1 > 0$ is often chosen as a diagonal matrix to simplify the design, i.e., $K_1 = \mathrm{diag}(k_{11}, k_{12}, k_{13})$, k_{1i} ($i = 1, 2, 3$) is constant value.

Now let us consider the Lyapunov function V_1, which is required positive definite around the desired position as follows:

$$V_1 = \frac{1}{2} z_1^T z_1 \,. \tag{21}$$

Step 2 (Backstepping for the variant of z_2)**.** Because there exists a dynamic error between the angular rate $\dot{\boldsymbol{\eta}}$ and its desired behavior of $\dot{\boldsymbol{\eta}}_r$, the speed tracking error vector for the attitude dynamics is defined as

$$z_2 \triangleq \dot{\boldsymbol{\eta}} - \dot{\boldsymbol{\eta}}_r = J\boldsymbol{\omega} - \alpha \quad . \tag{22}$$

and its derivative is

$$\dot{z}_2 = \ddot{\eta} - \ddot{\eta}_d + K_1 \dot{z}_1 \ . \tag{23}$$

Substituting (20) and (22) into (19) yields

$$\dot{z}_1 = z_2 + \alpha - \dot{\eta}_d = z_2 - K_1 z_1 \, . \tag{24}$$

that is,

$$z_2 = \dot{z}_1 + K_1 z_1 \ . \tag{25}$$

Differentiating (25) and substituting (18) yields

$$\dot{z}_2 = \ddot{\eta} - \ddot{\eta}_d + K_1 \dot{z}_1 \ . \tag{26}$$

From (20) and (24), the derivative of the stabilizing function α is

$$\dot{\alpha} = \ddot{\eta}_d - K_1 \left(z_2 - K_1 z_1 \right) = \ddot{\eta}_d - K_1 z_2 + K_1^2 z_1 \ . \tag{27}$$

The derivative of the first CLF of (21) can be rewritten as follows by substituting (24)

$$\dot{V}_1 = z_1^T \dot{z}_1 = z_1^T (z_2 - K_1 z_1) = -z_1^T K_1 z_1 + z_1^T z_2 \ . \tag{28}$$

Now a SMC control is introduced to improve system adaptiveness; the sliding surface *s* is defined first. The conventional linear sliding surface is designed as (Bolivar et al., 1997)

$$s_{B1} = \lambda_1 z_1 + \lambda_2 z_2 + \cdots + z_n \ , \tag{29}$$

where $z_i = \eta^{(i)} - \eta_r^{(i)}$ is the attitude error vector, $\eta^{(i)} = \dfrac{d^{(i)}\eta}{dt^{(i)}}$, i =1,2,…,n, the virtual angular vector of η_r meeting $\alpha = \dot{\eta}_r$, λ_1, λ_2,… are the control gains to be determined. By using this sliding surface, the associated Backstepping control law can be developed and called BSMC1 (Liu et al., 2020).

In this paper a new sliding surface is designed as (Bolivar and Zinober, 1994)

$$s_{B2} = z_n \tag{30}$$

the associated Backstepping design is called BSMC2. The sliding surface (30) is a simple relation comparing with s_{B1}, but the sliding manifold function s_{B2} is a combination of the primary error z_1 and its (n − 1) order

derivatives, such as Eq.(25). Therefore, for the 2nd and 3rd order systems, the sliding mode surfaces are designed as

$$s_{B2} = z_2 = \dot{z}_1 + K_1 z_1 , \tag{31.a}$$

By using the recursive construction form of the error variables in the backstepping procedure, $\dot{z}_i = -z_{i-1} - K_i z_i + z_{i+1}$, we get $\dot{z}_2 = -z_1 - K_2 z_2 + z_3$ and

$$s_{B3} = z_3 = \dot{z}_2 + K_2 z_2 + z_1 = \left(\ddot{z}_1 + K_1 \dot{z}_1\right) + K_2\left(\dot{z}_1 + K_1 z_1\right) + z_1 = \ddot{z}_1 + (K_1 + K_2) z_1 + K_2 K_1 z_1 + z_1 , \tag{31.b}$$

from (31) it can be seen that the sliding manifold function for BSMC2 is indeed a linear combination of the primary error z_1 and its $n-1$ derivatives. The essential difference of BSMC1 and BSMC2 is that the cross-coupling terms of all the z_i are canceled and the independence of the adjustment of the controller gains is improved for BSMC2 like in the pure backstepping case (Fossen and Strand, 1999). Although BSMC2 can not directly supports additional degree of freedom in the manifold parameter design as BSMC1, it can get good performances by using backstepping procedure and linear combination of the error and its $n-1$ derivatives.

The well known characteristics of SMC are attraction and invariance (Edwards and Spurgeon, 1998), that means the condition for the state to reach the sliding mode surface s in finite time t_r and remain it is

$$s\dot{s} < 0, \quad t < t_r \tag{32}$$

$$s = \dot{s} = 0, \; t \geq t_r \tag{33}$$

For the sliding mode surfaces of Eqs.(31), there are different reachability conditions, that are designed as (Bolivar and Zinober, 1994; Bolivar et al.,1997)

$$\dot{s}_{B_2} = -h_{B_{21}} z_1 - h_{B_{22}} s_{B_2} - \varsigma_{B_2} \mathrm{sgn}(s_{B_2}) , \tag{34}$$

so their corresponding attraction and invariance for the SMC are as follows,

$$s_{B_2} \dot{s}_{B_2} = -h_{B_{21}} z_2 z_1 - h_{B_{22}} z_2^2 - \varsigma_{B_2} |z_2| \tag{35}$$

where $h_{B_{21}}$, $h_{B_{22}}$, and ς_{B2} are sliding mode surface parameters with $h_{B_{21}} > 0$, $h_{B_{22}} > 0$, and $\varsigma_{B2} > 0$. Note that ς_{Bi}

can be chosen as small as possible to reduce the amplitude of the switching and h_{Bi} can be chosen to determine the time taken to attain sliding (Edwards C. and Spurgeon S.K., 1998).

Consider the unobservable disturbance $\boldsymbol{d}=\left[\boldsymbol{d}_V^T \quad \boldsymbol{d}_\omega^T\right]^T$, $\boldsymbol{d}_\omega$ is the associated attitude disturbance.

Assumption A1. Suppose that the unobservable disturbance d_ω varies slowly relative to the observer dynamics, i.e. $\dot{d}_\omega \approx 0$.

Remark 2. Literature shows that the method is also feasible for fast time-varying disturbances (Chen et al., 2000). In the presence of uncertainties, the unobservable disturbances would be a function of the states, which can be reasonably estimated if the disturbance observer dynamics are faster than that of the closed-loop system. The same argument for the state observer based control methods is available.

According to **Assumption A1** $\dot{d}_\omega \approx 0$, the derivative of the estimated parameter error is

$$\dot{\tilde{\boldsymbol{d}}}_\omega = \dot{\hat{\boldsymbol{d}}}_\omega - \dot{\boldsymbol{d}}_\omega = \dot{\hat{\boldsymbol{d}}}_\omega . \tag{36}$$

where $\hat{\boldsymbol{d}}_\omega$ and $\tilde{\boldsymbol{d}}_\omega$ are the estimated parameter vector of $\boldsymbol{d}_\omega$ and the associated estimated parameter error vector.

For the sliding mode surface s_{B2}, to meet the reachability (32) and (33), that is, denote $V_s = \frac{1}{2}s^T s$, substituting (26) into the derivative V_s yields

$$\dot{V}_s = \boldsymbol{z}_2^T \dot{\boldsymbol{z}}_2 = \boldsymbol{z}_2^T \left(\ddot{\boldsymbol{\eta}} - \ddot{\boldsymbol{\eta}}_d + K_1 \dot{\boldsymbol{z}}_1\right), \tag{37}$$

If the disturbance $\boldsymbol{d}$ is neglected, select $\ddot{\boldsymbol{\eta}} = -K_1 \dot{\boldsymbol{z}}_1 - h_{B_2} \boldsymbol{z}_2 - \varsigma_{B_2} \operatorname{sgn}(\boldsymbol{z}_2) + \ddot{\boldsymbol{\eta}}_d$, then

$$\begin{aligned} \dot{V}_s &= \boldsymbol{z}_2^T \left(-K_1 \dot{\boldsymbol{z}}_1 - h_{B_2} \boldsymbol{z}_2 - \varsigma_{B_2} \operatorname{sgn}(\boldsymbol{z}_2) + \ddot{\boldsymbol{\eta}}_d - \ddot{\boldsymbol{\eta}}_d + K_1 \dot{\boldsymbol{z}}_1\right) \\ &= -\boldsymbol{z}_2^T h_{B_2} \boldsymbol{z}_2 - \boldsymbol{z}_2^T \varsigma_{B_2} \operatorname{sgn}(\boldsymbol{z}_2) < 0, \end{aligned} \tag{38}$$

From kinematics equation (1), we get the desired angular accleration

$$\begin{aligned} \dot{\boldsymbol{\omega}} &\approx J^{-1}\left(\ddot{\boldsymbol{\eta}} - \dot{J}\boldsymbol{\omega}\right) \\ &= J^{-1}\left(-K_1 \dot{\boldsymbol{z}}_1 - h_{B_2} \boldsymbol{z}_2 - \varsigma_{B_2} \operatorname{sgn}(\boldsymbol{z}_2) + \ddot{\boldsymbol{\eta}}_d - \dot{J}\boldsymbol{\omega}\right) \end{aligned} \tag{39}$$

and according to dynamics equation of (12), we get

$$\dot{\boldsymbol{\omega}} \approx \boldsymbol{f}_{2\omega} + \boldsymbol{g}_{2\omega}\boldsymbol{n}_{CP} + \boldsymbol{g}_{3\omega}\boldsymbol{d}_{\omega} \tag{40}$$

Therefore, the associated control $\boldsymbol{n}_{CP}$ can be designed as

$$\begin{aligned}\boldsymbol{n}_{CP} &= \frac{1}{\boldsymbol{g}_{2\omega}}\left(-\boldsymbol{f}_{2\omega} - \boldsymbol{g}_{3\omega}\hat{\boldsymbol{d}}_{\omega} + \boldsymbol{J}^{-1}\left(-K_1\dot{z}_1 - h_{B_2}z_2 - \varsigma_{B_2}\,\mathrm{sgn}(z_2) + \ddot{\boldsymbol{\eta}}_d - \dot{\boldsymbol{J}}\boldsymbol{\omega}\right)\right) \\ &= \frac{1}{\boldsymbol{g}_{2\omega}}\left(-\boldsymbol{f}_{2\omega} - g_{3\omega}\hat{\boldsymbol{d}}_{\omega}\right) + \left(-K_1\dot{z}_1 - h_{B_2}z_2 - \varsigma_{B_2}\,\mathrm{sgn}(z_2) + \ddot{\boldsymbol{\eta}}_d - \dot{\boldsymbol{J}}\boldsymbol{\omega}\right)\end{aligned} \tag{41}$$

where $\hat{\boldsymbol{d}}_{\omega}$ is estimation of the attitude disturbance $\boldsymbol{d}_{\omega}$.

Since $\hat{\boldsymbol{d}}_{\omega} \neq \boldsymbol{d}_{\omega}$, $\ddot{\eta}$ needs to be redefined to meet $\dot{V}_s < 0$. Now selecting reachability condition as shown in (34) with consideration of disturbance estimation errors, we get

$$\dot{z}_2 = -\left(h_{B_{21}}z_1 + h_{B_{22}}z_2 + \varsigma_{B_2}\mathrm{sign}(z_2) + \boldsymbol{J}\boldsymbol{g}_{3\omega}\tilde{\boldsymbol{d}}_{\omega}\right), \tag{42}$$

Substitute (42) into (26) yields

$$\ddot{\boldsymbol{\eta}} = -K_1\dot{z}_1 + \ddot{\boldsymbol{\eta}}_d - \left(h_{B_{21}}z_1 + h_{B_{22}}z_2 + \varsigma_{B_2}\mathrm{sign}(z_2) + \boldsymbol{J}\boldsymbol{g}_{3\omega}\tilde{\boldsymbol{d}}_{\omega}\right) \tag{43}$$

By using (26), (43) we obtain

$$\begin{aligned}\dot{V}_s = s^T\dot{s} &= z_2^T\left(-K_1\dot{z}_1 + \ddot{\boldsymbol{\eta}}_d - \left(h_{B_{21}}z_1 + h_{B_{22}}z_2 + \varsigma_{B_2}\mathrm{sign}(z_2) + \boldsymbol{J}\boldsymbol{g}_{3\omega}\tilde{\boldsymbol{d}}_{\omega}\right) - \ddot{\eta}_d + K_1\dot{z}_1\right) \\ &= -z_2^T\left(h_{B_{21}}z_1 + h_{B_{22}}z_2 + \varsigma_{B_2}\mathrm{sign}(z_2) + \boldsymbol{J}\boldsymbol{g}_{3\omega}\tilde{\boldsymbol{d}}_{\omega}\right) \\ &= -s^T h_{B_{22}}s - s^T\left(h_{B_{21}}z_1 + \boldsymbol{J}\boldsymbol{g}_{3\omega}\tilde{\boldsymbol{d}}_{\omega} + \varsigma_{B_2}\mathrm{sign}(s)\right)\end{aligned} \tag{44}$$

The second term of the above equation can be rewritten as a function of the individual elements of the respective vectors (Vieira, 2019), denote $\hat{\varsigma}(z)I = \varsigma_{B_2}$, then (44) can be rewritten as

$$s^T\dot{s} = -s^T h_{B_{22}}s - \left[s_i\left(h_{B_{21}}^{ii}z_1^i + J_{ii}g_{3\omega}^i\tilde{\boldsymbol{d}}_{\omega}^i + \hat{\varsigma}(z)I\mathrm{sign}(s_i)\right)\right] \tag{45}$$

To ensure that $\dot{V}_s < 0$, it is necessary to select a time varying switch gain $\hat{\varsigma}(z_i)$, so define a critical gain $\bar{\varsigma} = \max(|z_{n-1} - \boldsymbol{J}\boldsymbol{g}_{3\omega}\tilde{\boldsymbol{d}}_{\omega}|) = \max(|z_1 - \boldsymbol{J}\boldsymbol{g}_{3\omega}\tilde{\boldsymbol{d}}_{\omega}|)$ and consider a positive scalar ς_0, it yields (Vieira, 2019)

$$s^T\dot{s}=-s^Ts-\left[s_i\left(h_{B_{21}}^{ii}z_1^i\right)+\left(\bar{\varsigma}+\varsigma_0\right)|s_i|\right]<0 \tag{46}$$

Hence the SMC invariance property can be guaranteed even under unknown disturbances.

From Eqs.(24) and (42), we obtain

$$\begin{bmatrix} h_{B_{21}} & 0 \\ 0 & I \end{bmatrix}\begin{pmatrix} \dot{\boldsymbol{z}}_1 \\ \dot{\boldsymbol{z}}_2 \end{pmatrix}=-\begin{bmatrix} h_{B_{21}}K_1 & 0 \\ 0 & h_{B_{22}} \end{bmatrix}\begin{pmatrix} \boldsymbol{z}_1 \\ \boldsymbol{z}_2 \end{pmatrix}+\begin{bmatrix} 0 & h_{B_{21}} \\ -h_{B_{21}} & 0 \end{bmatrix}\begin{pmatrix} \boldsymbol{z}_1 \\ \boldsymbol{z}_2 \end{pmatrix}-\begin{pmatrix} 0 \\ \varsigma_{B_2}\,\mathrm{sgn}(\boldsymbol{z}_2)+\boldsymbol{J}\boldsymbol{g}_{3\omega}\tilde{\boldsymbol{d}}_\omega \end{pmatrix} \tag{47}$$

Now the second augmented CLF is constructed as follows for BSMC2

$$V_2=\frac{1}{2}\begin{pmatrix} \boldsymbol{z}_1 \\ \boldsymbol{z}_2 \end{pmatrix}^T\begin{bmatrix} h_{B_{21}} & 0 \\ 0 & I \end{bmatrix}\begin{pmatrix} \boldsymbol{z}_1 \\ \boldsymbol{z}_2 \end{pmatrix}+\frac{1}{2\gamma_d}\tilde{\boldsymbol{d}}_\omega^T\tilde{\boldsymbol{d}}_\omega, \tag{48}$$

where γ_d is a positive constant that determines the convergence speed of the unobservable disturbance estimation. Substituting (47) into the derivative of (48) yields

$$\begin{aligned}\dot{V}_2&=\begin{pmatrix} \boldsymbol{z}_1 \\ \boldsymbol{z}_2 \end{pmatrix}^T\begin{bmatrix} h_{B_{21}} & 0 \\ 0 & I \end{bmatrix}\begin{pmatrix} \dot{\boldsymbol{z}}_1 \\ \dot{\boldsymbol{z}}_2 \end{pmatrix}+\frac{1}{\gamma_d}\tilde{\boldsymbol{d}}_\omega^T\dot{\tilde{\boldsymbol{d}}}_\omega \\ &=-\begin{bmatrix} \boldsymbol{z}_1 & \boldsymbol{z}_2 \end{bmatrix}\begin{bmatrix} h_{B_{21}}K_1 & 0 \\ 0 & h_{B_{22}} \end{bmatrix}\begin{pmatrix} \boldsymbol{z}_1 \\ \boldsymbol{z}_2 \end{pmatrix}-\varsigma_{B_2}\|\boldsymbol{z}_2\|_1-\boldsymbol{z}_2^T\boldsymbol{J}\boldsymbol{g}_{3\omega}\tilde{\boldsymbol{d}}_\omega+\frac{1}{\gamma_d}\tilde{\boldsymbol{d}}_\omega^T\dot{\tilde{\boldsymbol{d}}}_\omega\end{aligned} \tag{49}$$

where $\|x\|_1=\sum_{i=1}^{n}|x_i|$. By using (36) and $s^T\tilde{\boldsymbol{d}}_\omega=\tilde{\boldsymbol{d}}_\omega^Ts$, we obtain

$$-\boldsymbol{z}_2^T\boldsymbol{J}\boldsymbol{g}_{3\omega}\tilde{\boldsymbol{d}}_\omega+\frac{1}{\gamma_d}\tilde{\boldsymbol{d}}_\omega^T\dot{\tilde{\boldsymbol{d}}}_\omega=-\tilde{\boldsymbol{d}}_\omega^T\left(\boldsymbol{J}\boldsymbol{g}_{3\omega}\right)^T\boldsymbol{z}_2+\frac{1}{\gamma_d}\tilde{\boldsymbol{d}}_\omega^T\dot{\tilde{\boldsymbol{d}}}_\omega \tag{50}$$

Choose the update law as:

$$\dot{\tilde{\boldsymbol{d}}}_\omega=\gamma_d\boldsymbol{g}_{3\omega}^T\boldsymbol{J}^T\boldsymbol{z}_2, \tag{51}$$

substitute (51) into (49) yields

$$\dot{V}_2=-\begin{bmatrix} \boldsymbol{z}_1 & \boldsymbol{z}_2 \end{bmatrix}\begin{bmatrix} h_{B_{21}}K_1 & 0 \\ 0 & h_{B_{22}} \end{bmatrix}\begin{pmatrix} \boldsymbol{z}_1 \\ \boldsymbol{z}_2 \end{pmatrix}-\varsigma_{B_2}\|\boldsymbol{z}_2\|_1<0. \tag{52}$$

Therefore, robust stability of the closed-loop system can be guaranteed by using the DO-BSMC controller

according to Lyapunov theory. The associated $\dot{\omega}_d$ can be obtained from (40) and (41).

From the above analysis, the structure of the adaptive integral backstepping controller for attitude control can be designed as Fig.2, which includes attitude dynamics of the airship and adaptive sliding mode backstepping control with an adaptive disturbance estimator.

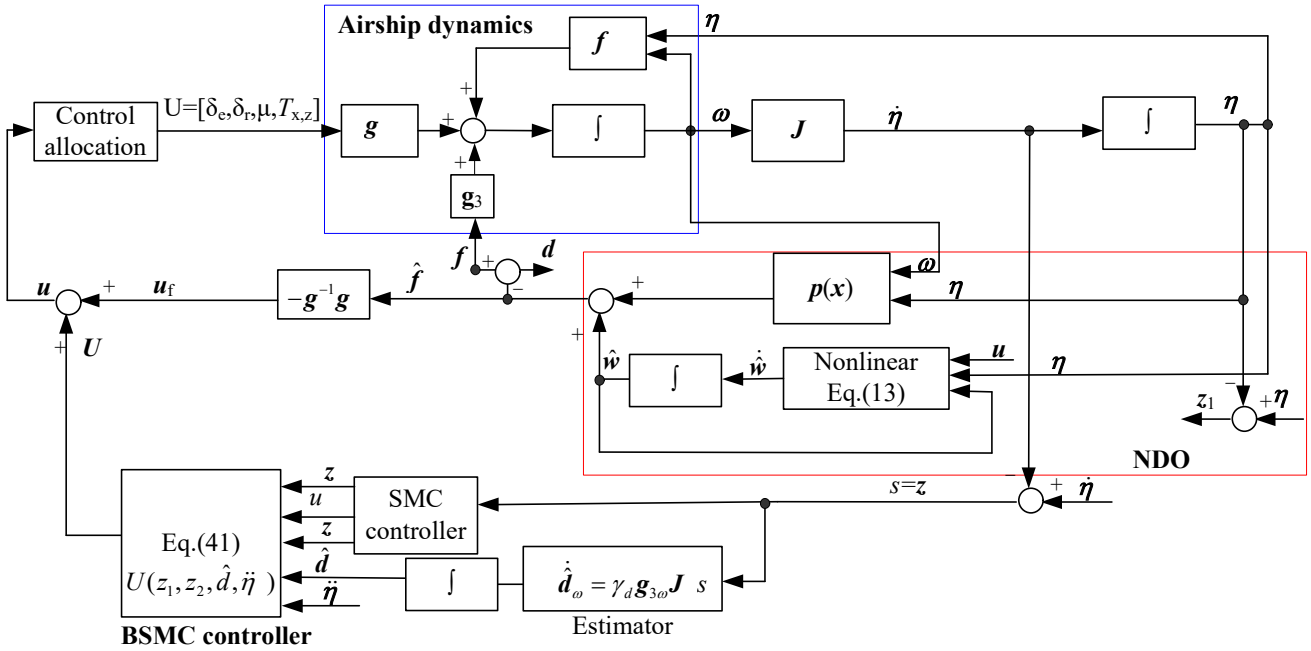

Fig.2 Block diagram of the adaptive sliding mode backstepping controller

3.3 Velocity Control Based on CLF

This section is to design a backstepping velocity controller, and the objective is to make the airspeed υ_a of the airship converge to the desired values $\upsilon_{a,d}$. The velocity can be controlled directly via the acceleration of the airship. Now the velocity tracking error vector is defined as

$$z_3 \triangleq \upsilon_a - \upsilon_d \tag{53}$$

where $\upsilon_a = \begin{bmatrix} u & v & w \end{bmatrix}^T$. The associated CLF is chosen as

$$V_3 = \frac{1}{2} z_3^T z_3 . \tag{54}$$

According to Lyapunov theory, $\dot{V}_3$ is required to be semi-negative definite (that is, $\dot{V}_3 = -K_3 z_3^T z_3$). To ensure

the closed-loop system stability, the desired linear acceleration vector is set using (54):

$$\dot{\boldsymbol{\upsilon}}_{a,d} = \dot{\boldsymbol{\upsilon}}_d - K_3 \boldsymbol{z}_3 = \dot{\boldsymbol{\upsilon}}_d + K_3 \boldsymbol{\upsilon}_d - K_3 \boldsymbol{\upsilon}_a \tag{55}$$

where control gain matrices $K_3 = \mathrm{diag}(k_{31}, k_{32}, k_{33}) > 0$. k_{31} , k_{32} and k_{33} are constant, and $\dot{\upsilon}_{a,d}$ denotes desired linear acceleration vector in $\mathbf{F}_\mathrm{b}$.

Once all of the control laws of the desired linear accelerations and angular accelerations are obtained, the associated control forces and moments can be achieved by the following equation:

$$\boldsymbol{U} = M_a \dot{\boldsymbol{V}} - \boldsymbol{F}_k - \boldsymbol{F}_w - \boldsymbol{F}_{GB} - \boldsymbol{F}_A . \tag{56}$$

To obtain the practical control surfaces and thruster inputs, a control allocation problem is presented to solve (9) with actuator saturation constraints, the control allocation problem can be solved as in Liu and Sang (2018). When the optimal solution $\boldsymbol{u}^*$ is found, the practical control input signals, including thrust, tilt angle and control surface deflections, are obtained.

3.4 The trajectory guider controller

The objective of the trajectory guider is to generate the desired attitude and velocity commands. It is described in this section. The trajectory guider controller has to calculate the desired attitudes and speeds in the x – and z–directions such that the airship follows the desired path despite the inability to exert direct control over the speed in the y-direction. According to the virtual spring damping principle, the desired or commanded velocity $\dot{\upsilon}_c$ in $\mathbf{F}_g$ is first obtained by the following differential equation as in Liu and Sang (2018). It can be seen that perfect tracking without wind requires that $\dot{\boldsymbol{r}}_g = \boldsymbol{\upsilon}_g = \boldsymbol{\upsilon}_c = \dot{\xi}$, and the desired attitude η_d and velocity υ_d in the body-fixed frame are generated by using kinematics relation and the command velocity of υ_c , the detailed design procedure of the high-level controller is in Liu and Sang (2018), so is not described here.

3.5 Stability Analysis

Lemma 1. (Fossen, 1994) Consider the nonlinear system $\dot{\boldsymbol{x}}(t) = f(\boldsymbol{x})$ with the equilibrium point $\boldsymbol{x}^*$. Let $V(x): \mathbb{C} \to \mathbb{R}$ be a continuously differentiable function such that for $\boldsymbol{x} \in \mathbb{C}$ ($\mathbb{C} \subset \mathbb{R}^n$)

1) $V(\boldsymbol{x}) > 0$ (positive definite) with $\dot{V}(\boldsymbol{x}) < 0$ (negative definite),

2) $V(\boldsymbol{x}) \to \infty$ as $\|\boldsymbol{x}\|^2 \to \infty$ (radially unbounded),

then the equilibrium point $\boldsymbol{x} = 0$ satisfying f($\boldsymbol{x}^*$) = 0 is globally asymptotically stable.

Assumption A2. The reference trajectory $\boldsymbol{\xi}_r(t)$: $[0,\infty) \to \mathbb{R}^3$ is sufficiently smooth with its time-derivatives ($\boldsymbol{\upsilon}_r(t) = \dot{\boldsymbol{\xi}}_r(t)$, $\dot{\boldsymbol{\upsilon}}_r(t)$) bounded.

Because the trajectory tracking control is based on guidance, the control objective of the speed loop is that the guidance-based command signal $\boldsymbol{\upsilon}_c(t)$ can be tracked by the system output of velocity $\dot{\boldsymbol{\xi}}(t)$.

Assumption A3. The output signal $\dot{\boldsymbol{\xi}}(t)$ or $\dot{\boldsymbol{r}}_g(t)$ tracks the commanded signal $\boldsymbol{\upsilon}_c(t)$ in (58) without steady tracking error, i.e., $\lim_{t\to\infty} \dot{\boldsymbol{\xi}}(t) = \lim_{t\to\infty} \boldsymbol{\upsilon}_c(t)$ with $\dot{\boldsymbol{\xi}}(t) = \boldsymbol{R}(\boldsymbol{\eta})\boldsymbol{\upsilon}_a$.

Theorem 1. Consider the system of (1) and (12) with Assumption A2 and A3 being satisfied. If there exist appropriately dimensional diagonal matrices of K_1, K_3, λ_1, constant parameters of $h_{B_{21}}$, $h_{B_{22}}$, ς_{B2}, γ_d, and sufficiently small scalar parameter ε, such that $K_1 > 0$, $K_3 > 0$, $h_{B_{21}} > 0$, $h_{B_{22}} > 0$, and $\varsigma_{B2} > 0$, γ_d meeting with (48), $\varepsilon \le \min\{\sqrt{\sigma_1\sigma_2}, 4\sigma_1\sigma_2/(4\sigma_1+\sigma_2)\}$,then the DO-BSMC control, given by (16), (41) and (56), can guarantee the requirements of 1) and 2) in section 2.3.

Proof.

Define the tracking error of position and velocity for the trajectory guider controller as $z_4 \triangleq \begin{pmatrix} \boldsymbol{\xi} - \boldsymbol{\xi}_r \\ \boldsymbol{\upsilon}_c - \boldsymbol{\upsilon}_r \end{pmatrix}$. A Lyapunov function for the entire system is established in accordance with (48) and (54):

$$V = V_l + V_h = \left(\frac{1}{2} \begin{pmatrix} z_1 \\ z_2 \end{pmatrix}^T \begin{bmatrix} h_{B_{21}} & 0 \\ 0 & I \end{bmatrix} \begin{pmatrix} z_1 \\ z_2 \end{pmatrix} + \frac{1}{2\gamma_d} \tilde{\boldsymbol{d}}_\omega^T \tilde{\boldsymbol{d}}_\omega + \frac{1}{2} z_3^T z_3 \right) + \frac{1}{2} z_4^T P z_4 \ , \tag{57}$$

where $\boldsymbol{z}_i$ (i = 1, 2, 3, 4) are the tracking error vectors defined in Section 3.1 and 3.2, P is positive definite for sufficiently small values of ε, and the Lyapunov function in (57) is chosen for the high-level controller as:

$$V_h \triangleq \frac{1}{2}\boldsymbol{z}_4^T P \boldsymbol{z}_4 \ , \tag{58}$$

where

$$P = \begin{pmatrix} 1 & \dfrac{\varepsilon}{\sigma_1\sigma_2} \\ \dfrac{\varepsilon}{\sigma_1\sigma_2} & \dfrac{1}{\sigma_1\sigma_2} \end{pmatrix}, \tag{59}$$

Then the derivative with respect to time of (58) can be obtained by using (59)

$$\dot{V}_h = \frac{1}{2}\boldsymbol{z}_4^T \left[\begin{pmatrix} 0 & -\sigma_1\sigma_2 \\ 1 & -\sigma_2 \end{pmatrix} P + P \begin{pmatrix} 0 & 1 \\ -\sigma_1\sigma_2 & -\sigma_2 \end{pmatrix} \right] \boldsymbol{z}_4 \triangleq -\boldsymbol{z}_4^T \bar{Q} \boldsymbol{z}_4 \le 0 \ , \tag{60}$$

where $\bar{Q} = \begin{pmatrix} \varepsilon & \dfrac{\varepsilon}{2\sigma_1} \\ \dfrac{\varepsilon}{2\sigma_1} & \dfrac{\sigma_2 - \varepsilon}{\sigma_1\sigma_2} \end{pmatrix}$. Substituting (52), and (54) into the derivative of (57) yields

$$\begin{aligned} \dot{V} &= \begin{bmatrix} \boldsymbol{z}_1 & \boldsymbol{z}_2 \end{bmatrix} \begin{bmatrix} h_{B_{21}} K_1 & 0 \\ 0 & h_{B_{22}} \end{bmatrix} \begin{pmatrix} \boldsymbol{z}_1 \\ \boldsymbol{z}_2 \end{pmatrix} - \varsigma_{B_2} \left\| \boldsymbol{z}_2 \right\|_1 + \boldsymbol{z}_3^T (\dot{\upsilon} - \dot{\upsilon}_d) - \boldsymbol{z}_4^T \bar{Q} \boldsymbol{z}_4 \\ &\triangleq -\boldsymbol{z}^T \Lambda_2 \boldsymbol{z} - \varsigma_{B_2} \left\| \boldsymbol{z}_2 \right\|_1 \\ &\le -\boldsymbol{z}^T \Lambda_2 \boldsymbol{z} \\ &\le -\lambda_{\min}(\Lambda_2) \boldsymbol{z}^T \boldsymbol{z} \ , \end{aligned} \tag{61}$$

where $\Lambda_2 = \mathrm{diag}\left(h_{B_{21}} K_1, h_{B_{22}}, K_3, \bar{Q} \right)$, and λ_{min} (Λ_2) is the minimum eigenvalue of Λ_2. $\boldsymbol{z}^T = \begin{bmatrix} \boldsymbol{z}_1^T & \boldsymbol{z}_2^T & \boldsymbol{z}_3^T & \boldsymbol{z}_4^T \end{bmatrix}$. For sufficiently small value of ε less than $\min\{\sqrt{\sigma_1\sigma_2}, 4\sigma_1\sigma_2/(4\sigma_1+\sigma_2)\}$, then $\bar{Q} > 0$, $K_1 > 0$, $K_3 > 0$, $h_{B_{21}} > 0$, $h_{B_{22}} > 0$, and $\varsigma_{B2} > 0$, so Λ_2 is positive definite, and $\dot{V}$ is negative definite. According to Lemma 1, the system is globally asymptotically stable at $\boldsymbol{z} = \boldsymbol{0}$. Thus, the reference trajectory $\boldsymbol{\xi}_r$ is precisely

tracked with $\lim_{t\to\infty}\left\|\boldsymbol{\xi}(t)-\boldsymbol{\xi}_r(t)\right\|=0$.

4. Simulation and Analysis

The considered model is a 250m length, 75m diameter airship, and the structure parameters and aerodynamic coefficients of the stratospheric airship are listed in Table 1.

Scenario I: Trajectory tracking control under unknown external disturbance.

In this case suppose that there is the unknown disturbance vector *f* acting on the airship, given by

$$\boldsymbol{f}(t) = [0.4, -0.5, 0.4, 0.05, 0.1, 0.1]^{\mathrm{T}} \tag{62}$$

where the units are m/s^2 for linear acceleration and rad/s^2 for angular acceleration respectively.

The gains of the disturbance observer (13) are designed as

$$l(x) = \mathrm{diag}([2.6\ 0.0088\ 1.8\ 0.5\ .198\ 1]), \quad \text{(BSMC1)} \tag{63.a}$$

$$l(x) = \mathrm{diag}([7.8\ 0.008\ 2.4\ 1.8\ 0.275\ 0.45]), \quad \text{(BSMC2)} \tag{63.b}$$

To illustrate our method in attitude control, a control design, the controller parameters are designed as follows

$$\begin{aligned}&\sigma_1 = 0.1\ \left[\frac{1}{\mathrm{s}}\right], \sigma_2 = 0.2\ \left[\frac{1}{\mathrm{s}}\right], c_\psi = 12\ \left(\frac{\mathrm{deg}\cdot\mathrm{s}}{\mathrm{m}}\right),\\ &K_1 = 0.5I_3, K_3 = 4I_3, W_v = I_6, \quad \text{(BSMC2)}\\ &W_u = I_6, \gamma_d = 0.2, h_{B_2} = \varsigma_{B_2} = 1, \zeta = 0.4, \varepsilon_0 \to 0\end{aligned} \tag{64}$$

To analyze the DO-BSMC2 control performance, the BSMC1 (Liu et al., 2020) with disturbance observer is used to compare, where the parameters of DO-BSMC1 are designed as follows,

$$\begin{aligned}&\sigma_1 = 0.1\ \left[\frac{1}{\mathrm{s}}\right], \sigma_2 = 0.2\ \left[\frac{1}{\mathrm{s}}\right], c_\phi = 1\ \left(\frac{\mathrm{deg}\cdot\mathrm{s}}{\mathrm{m}}\right), c_\psi = 12\ \left(\frac{\mathrm{deg}\cdot\mathrm{s}}{\mathrm{m}}\right),\\ &K_1 = 0.5I_3, \lambda_1 = 0.5I_3, K_3 = 4I_3, W_v = I_5, W_u = I_6, \quad \text{(BSMC1)}\\ &\gamma_d = 0.2, h_{B_1} = 1, \varsigma_{B_1} = 1, \zeta = 0.4, \varepsilon_0 \to 0\end{aligned} \tag{65}$$

where K_1 and K_3 are chosen to meet the requirements 1) and 2) in Section 2 through iterative design. I_i denotes the $i \times i$ unit matrix, i =3, 6.

The position range for the actuators are $[-25, 25](°)$, and their rate is confined in $[-80, 80](°/s)$. The initial position $\boldsymbol{\xi}_0 = [0, 0, -20000]^{\mathrm{T}}$ (m), and initial body velocity $\boldsymbol{\upsilon}_0 = [18,0,0]^{\mathrm{T}}$ (m/s), initial attitude $\boldsymbol{\eta}_0 = [0, 0, 0]^{\mathrm{T}}$, and initial angular velocity $\boldsymbol{\omega}_0 = [0, 0, 0]^{\mathrm{T}}$.

To validate the trajectory tracking control performance of the DO-BSMC design, a helix reference trajectory function is defined as

$$\boldsymbol{\xi}_r(t) = [x_r, y_r, z_r]^T \triangleq \int_0^t \dot{\boldsymbol{\xi}}_r(t)d\tau + \boldsymbol{\xi}_{r0} \ , \tag{66}$$

where the reference velocity $\dot{\boldsymbol{\xi}}_r(t) = \upsilon_r = [V_h \cos(\frac{2\pi}{T}t), V_h \sin(\frac{2\pi}{T}t), -V_z]^T$ and its initial reference position $\boldsymbol{\xi}_{r0} = [40, -50, -19960]^T$ (m). The horizontal tracking speed $V_h = 20$ m/s, the ascending speed is $V_z = 1$ (m/s), and the motion period $T = 300$ (s).

The simulation results are shown in Fig.3-Fig.8.

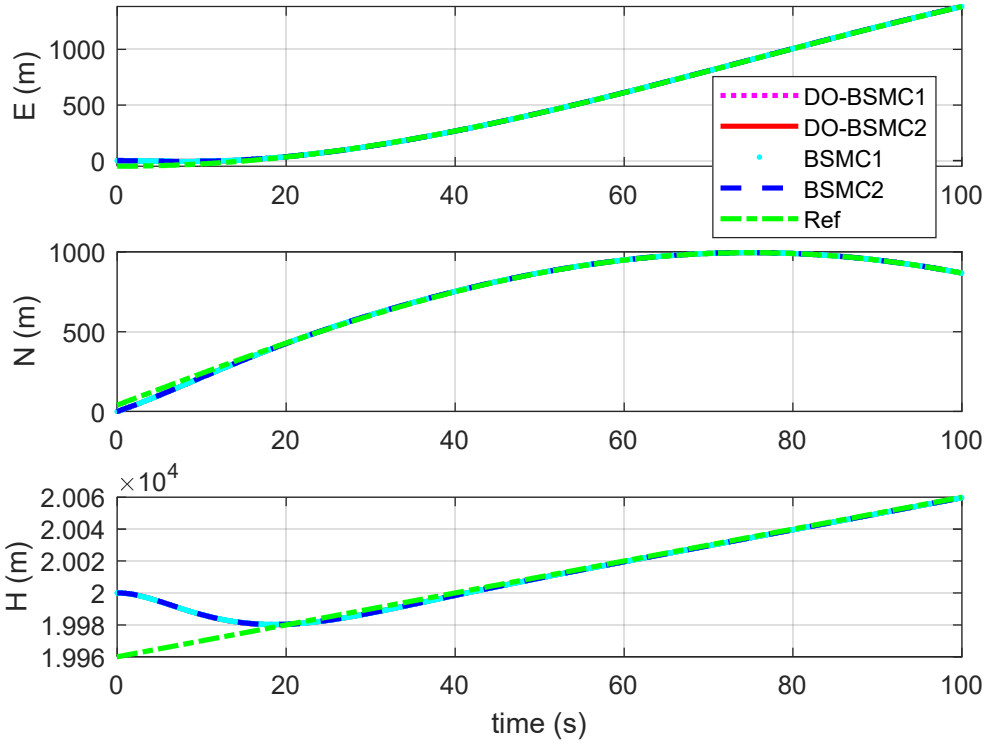

Fig. 3. Position tracking responses with disturbance inputs

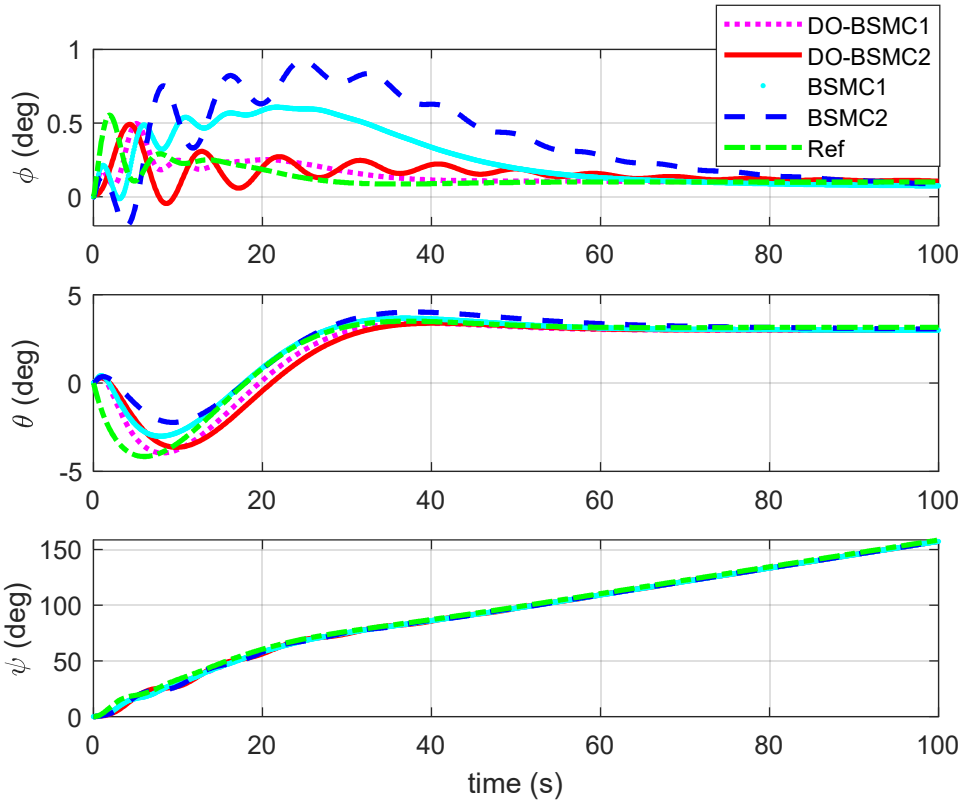

Fig. 4. Attitude angles tracking responses with disturbance inputs

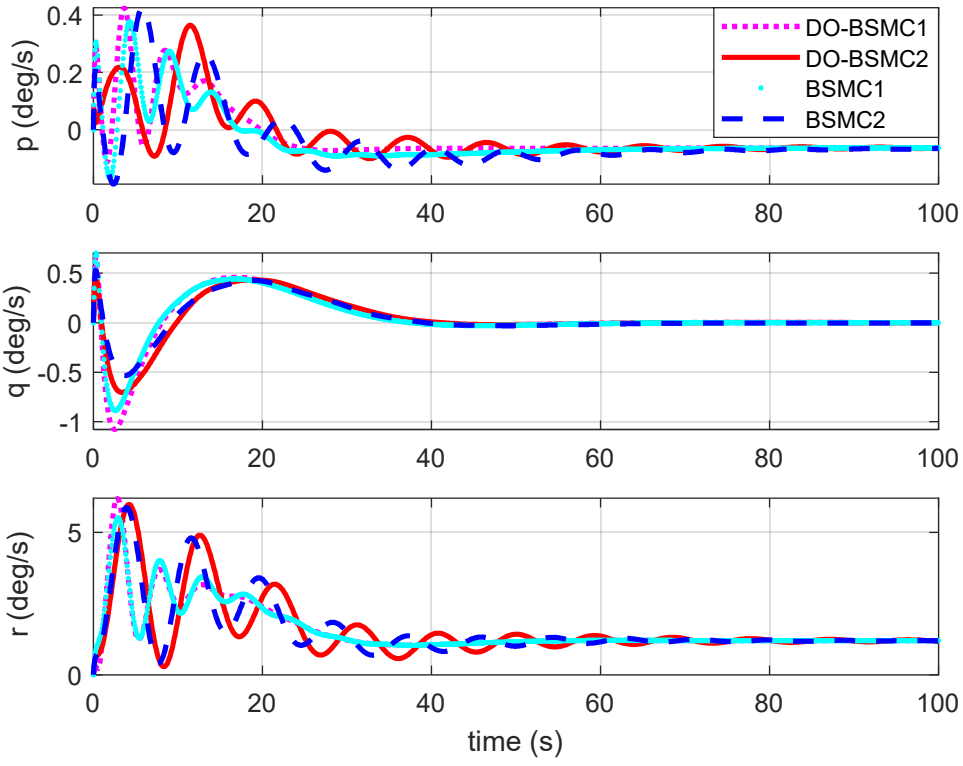

Fig. 5. Angular rate tracking responses with unknown disturbance inputs

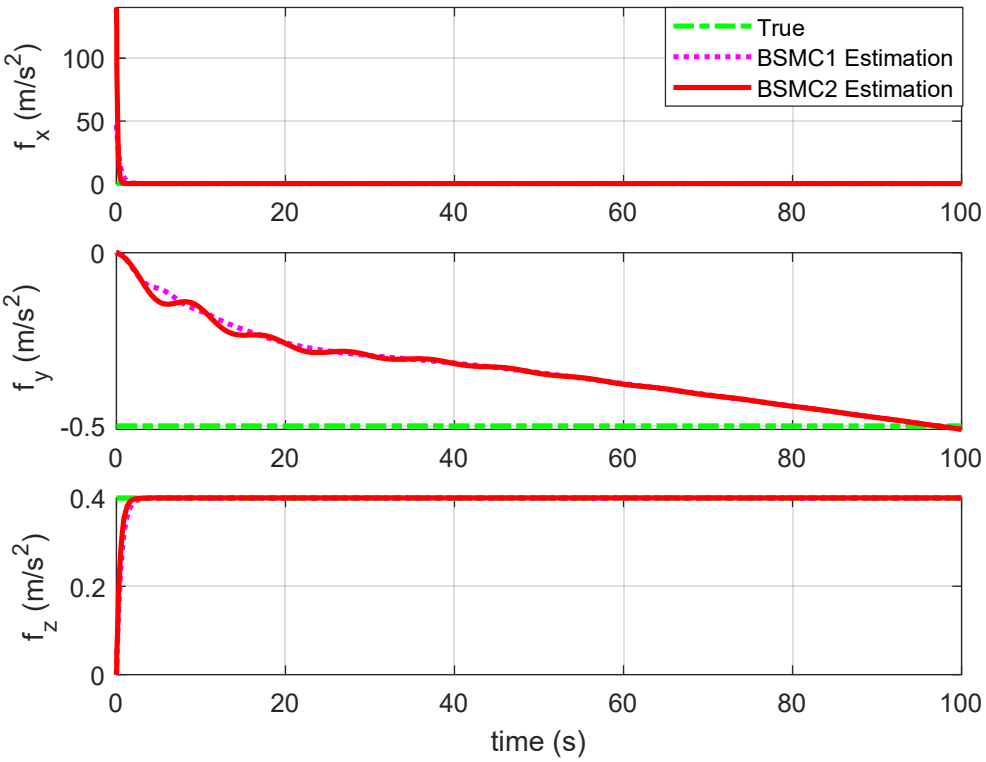

Fig. 6. Estimation of the observable position disturbances

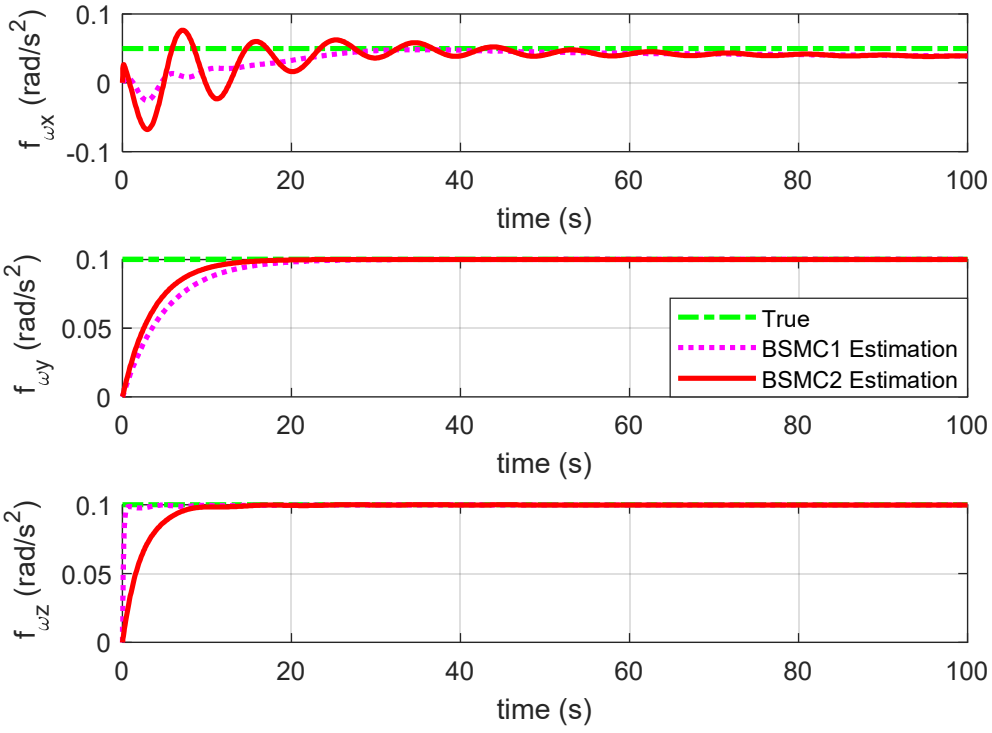

Fig. 7. Estimation of the observable attitude disturbances

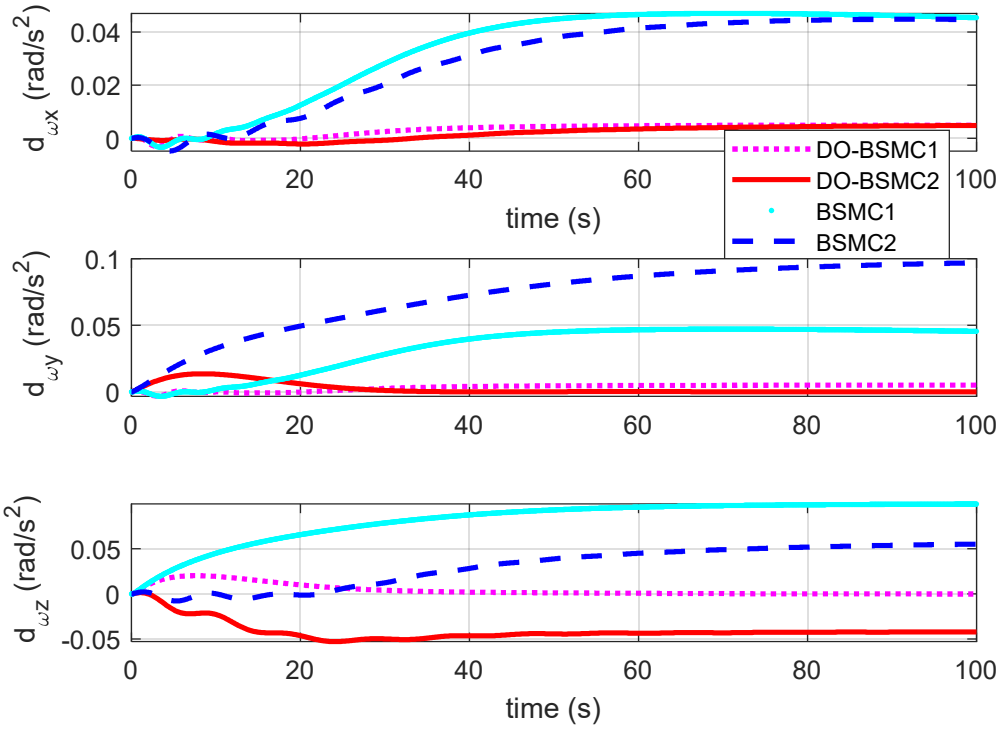

Fig. 8. Estimation of unobservable attitude disturbances

From Fig.3-4, it is clear that the reference trajectory and attitudes have been accurately tracked using the DO-BSMC2 method and the tracking errors converge to the desired position and attitude within 60 seconds, even in the presence of unknown disturbances. For the roll motion response there are some oscillations because of weak roll damping of the airship, so the convergence time is longer. Comparing with the BSMC, the proposed DO-BSMC control has lower tracking errors in attitude and position responses, which shows DO-BSMC control has more capability to deal with unknown disturbances for the airship. Comparison with BSMC1, responses of BSMC2 have more tracking errors and larger fluctuating in roll motion, so the linear sliding surface (29) applies position feedback and improves the output tracking performances. From Fig.5 the tracking roll rate and yaw rate responses have small **oscillations**, **and amplitudes of oscillations of the BSMC1 and BSMC2 tracking responses are more than those of the DO-BSMC1 and DO-BSMC2, meanwhile attenuation speeds of the BSMC1 tracking responses are fast than those of the BSMC2 tracking responses.** Figures 6 and 7 show the observable disturbance vector can be accurately estimated by

the NDO of (13) although there are some errors in the transition phase. Fig.8 shows the unobservable attitude disturbances have been adaptively estimated by the observer (51), and the responses of DO-BSMC have smaller overshoots and are faster converging than those of the BSMC design, which show DO can improve the tracking performances and disturbance rejection levels.

Scenario II: Trajectory tracking control under parameter uncertainty and unknown disturbances

This scenario considers model parameter uncertainty due to aerodynamic derivatives varying accordingly with angle of attack (AOA). So aerodynamic coefficients are set as follows

$$\begin{bmatrix} \Delta f_x \\ \Delta f_y \\ \Delta f_z \\ \Delta f_{mx} \\ \Delta f_{my} \\ \Delta f_{mz} \end{bmatrix} = \begin{bmatrix} (1.3+0.5\alpha)C_x \\ (1.3+0.5\alpha)C_y \\ (1.3-0.5\alpha)C_z \\ (0.7-0.5\alpha)C_{mx} \\ (0.7-0.5\alpha)C_{my} \\ (0.7-0.5\alpha)C_{mz} \end{bmatrix}, \tag{67}$$

where $\triangle$ denotes perturbation value. In this scenario the parameter uncertainty and external disturbances are considered simultaneously.

The reference trajectory function is the same as Scenario I. To compare control performances, Scenario II is simulated by using the BSMC2 with the same parameters as (64) ~ (65) in the three channels of roll, pitch and yaw. Meanwhile the parameters in the guidance loop are chosen as (64) ~ (65). The trajectory tracking responses are shown in Fig.9 and Fig.10. From Fig.10, it can be seen that responses of attitude angles for BSMC without the NDO estimation have more overshoot and bigger steady tracking errors than those for the DO-BSMC method, which shows the DO-BSMC design has more adaptive capability for aerodynamic coefficient uncertainty and unknown disturbances environment. Meanwhile, the roll responses are fluctuating with small amplitude, see Fig.10, the reason is low damping in the roll motion.

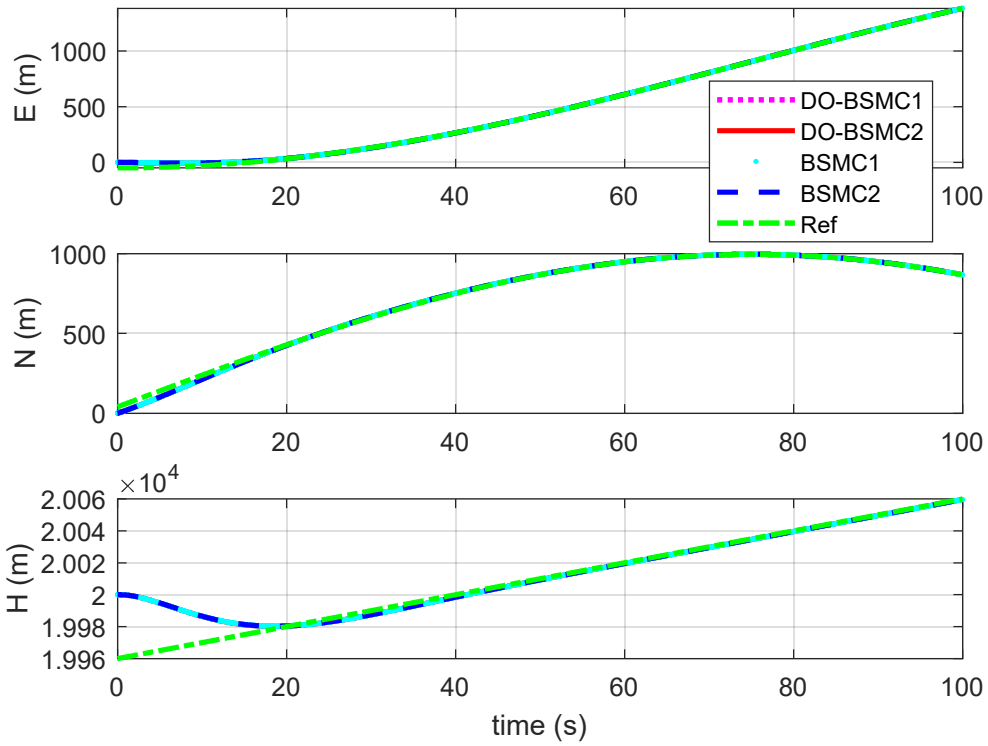

Fig.9. Position tracking responses with model uncertainty and unknown disturbances

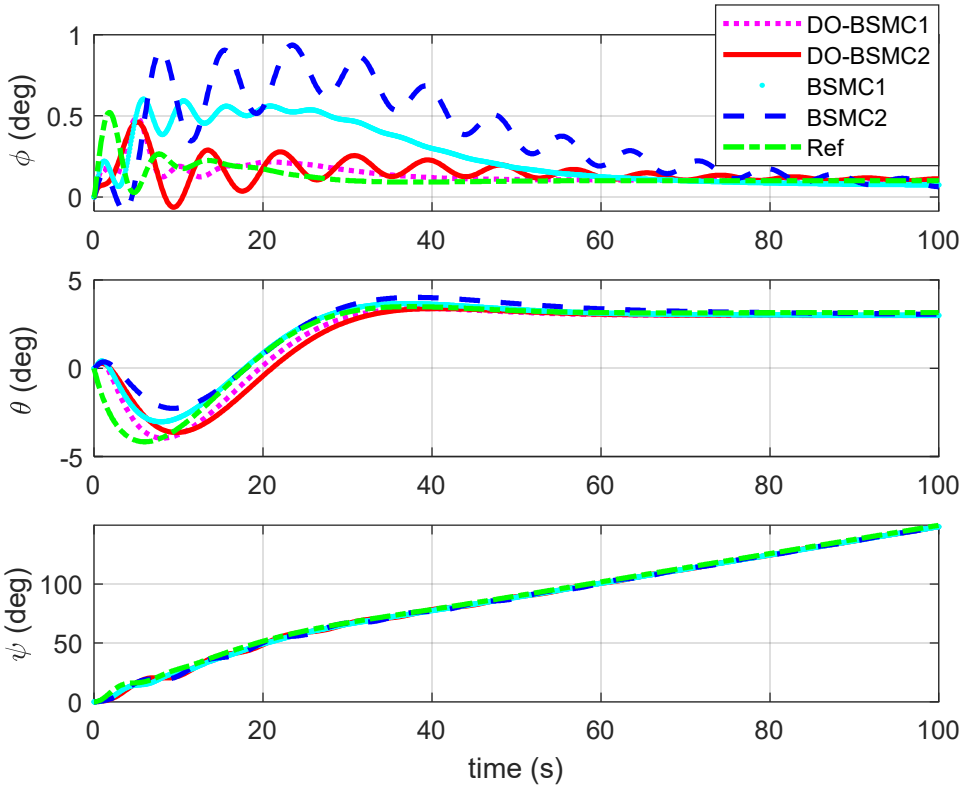

Fig.10. Euler angle tracking responses with model uncertainty and unknown disturbances.

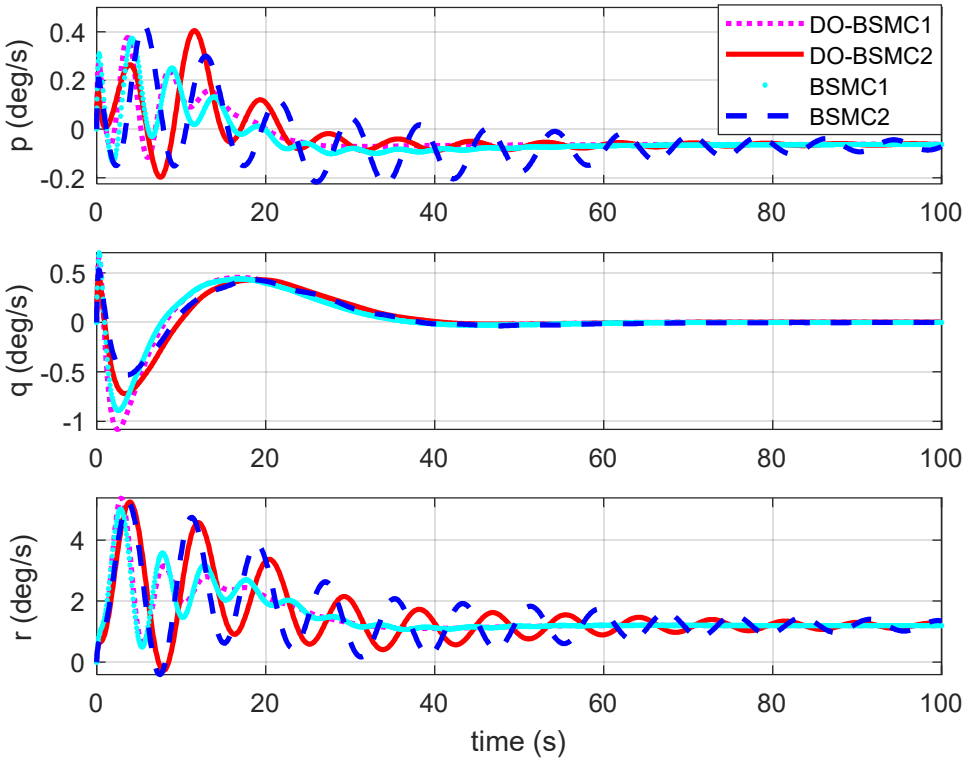

Fig.11 Angular rate tracking responses with model uncertainty and unknown disturbances

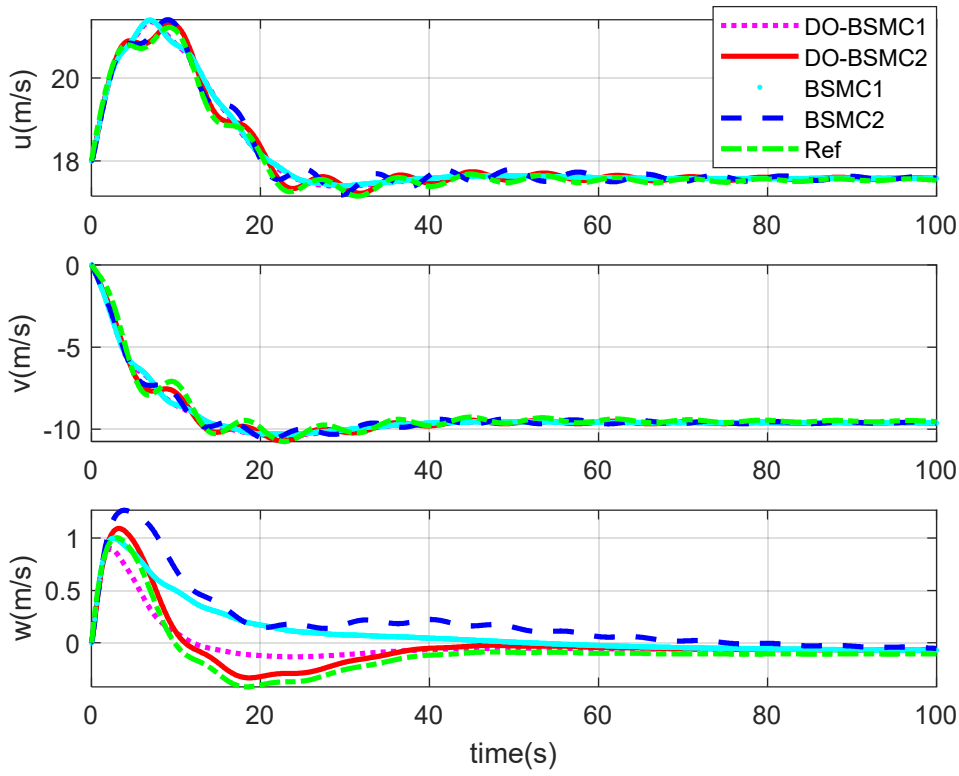

Fig.12 Flight speed responses with model uncertainty and unknown disturbances

From Fig.11 the tracking roll rate and yaw rate responses have small oscillations due to small damping, **and amplitudes of oscillations of the BSMC1 and BSMC2 tracking responses are more than those of the DO-BSMC1 and DO-BSMC2, meanwhile attenuation speeds of the BSMC1 tracking responses are fast than those of the BSMC2 tracking responses.** From Fig.12, it can be seen that speed responses of the DO-BSMC have less overshoot than those of the BSMC design due to the disturbance estimation effect. Figures 13 and 14 show the observable disturbance vector can be accurately estimated by the NDO of (13) although there are some errors in the transition phase. Fig.15 shows the unobservable attitude disturbances have been adaptively estimated, and the responses of DO-BSMC have smaller overshoots and are faster converging than those of the BSMC design, which show DO can improve the tracking performances and disturbance rejection levels.

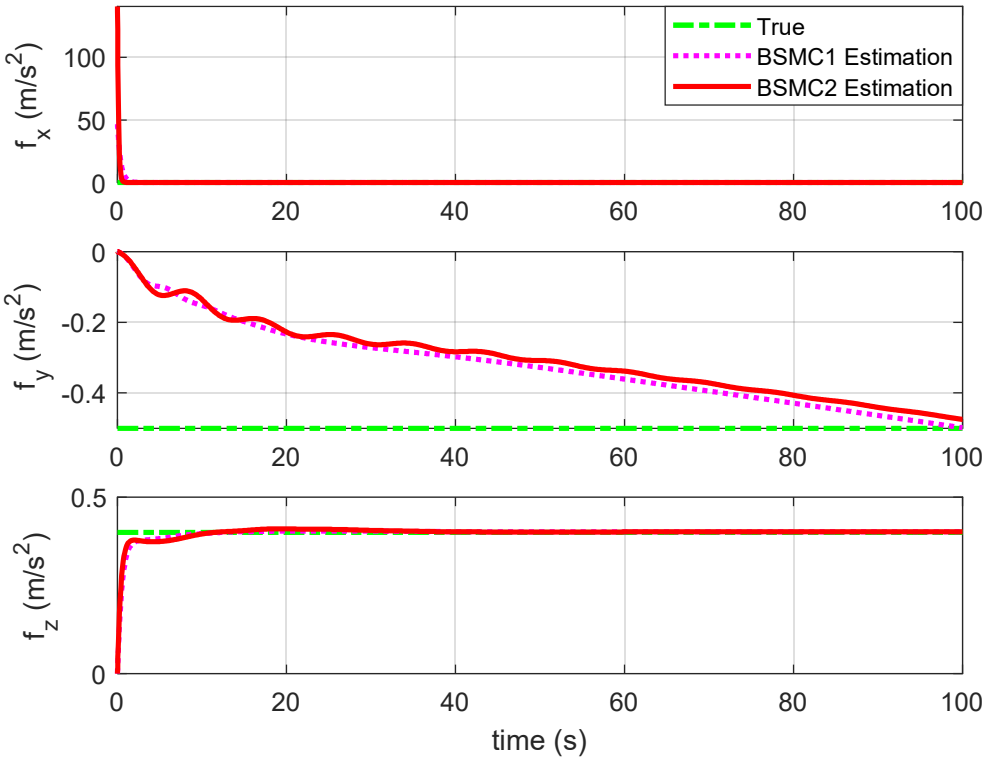

Fig. 13. Estimation of the observable position disturbances

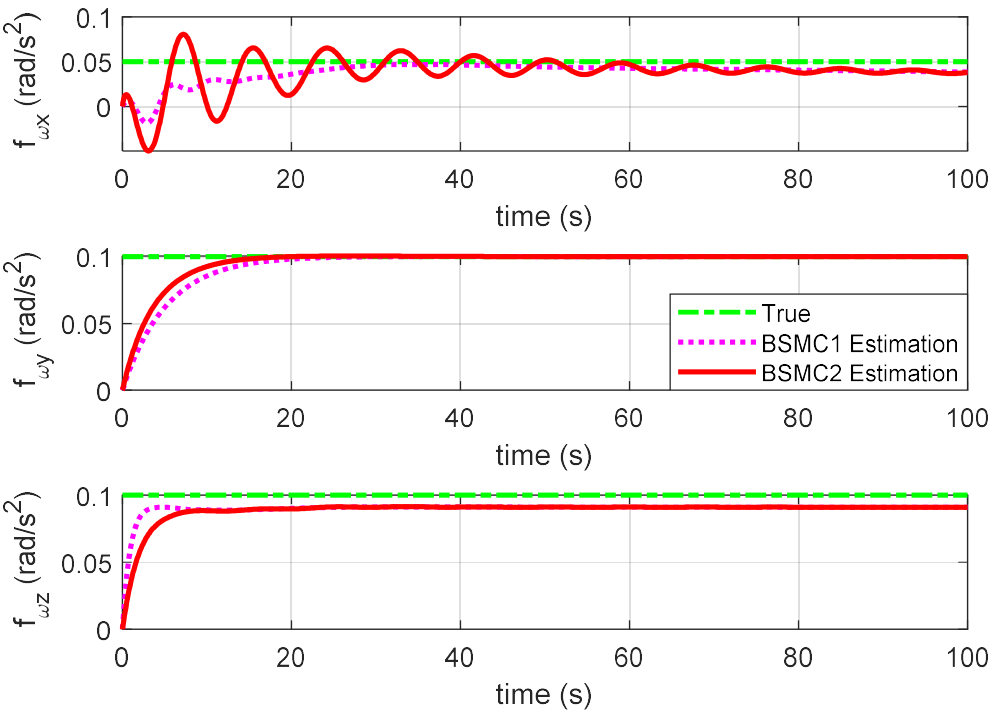

Fig. 14. Estimation of the observable attitude disturbances

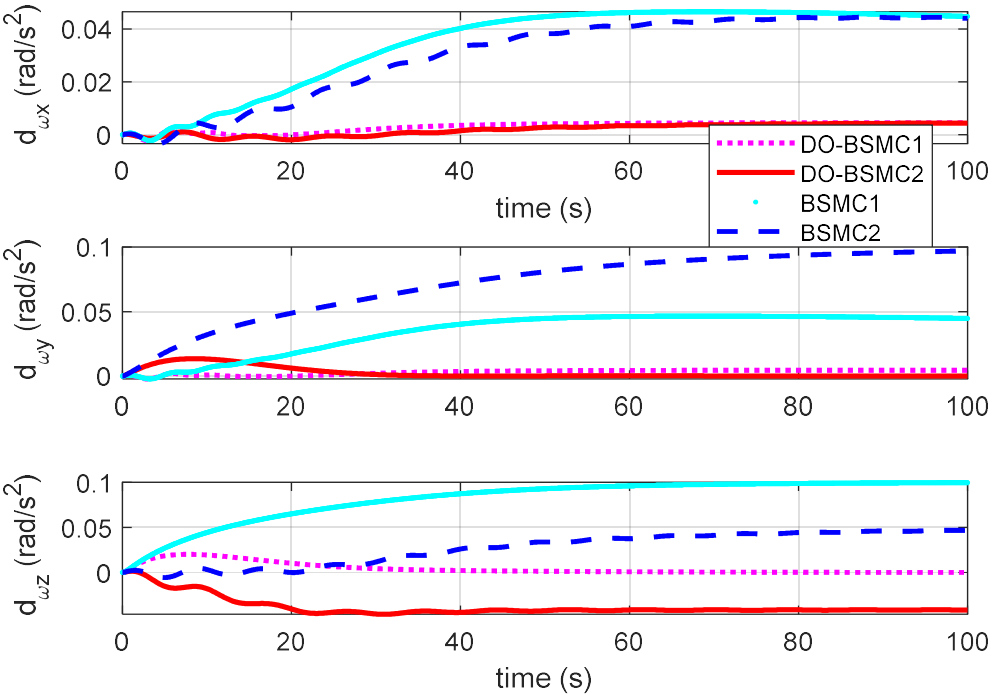

Fig. 15. Estimation of the unobservable attitude disturbances

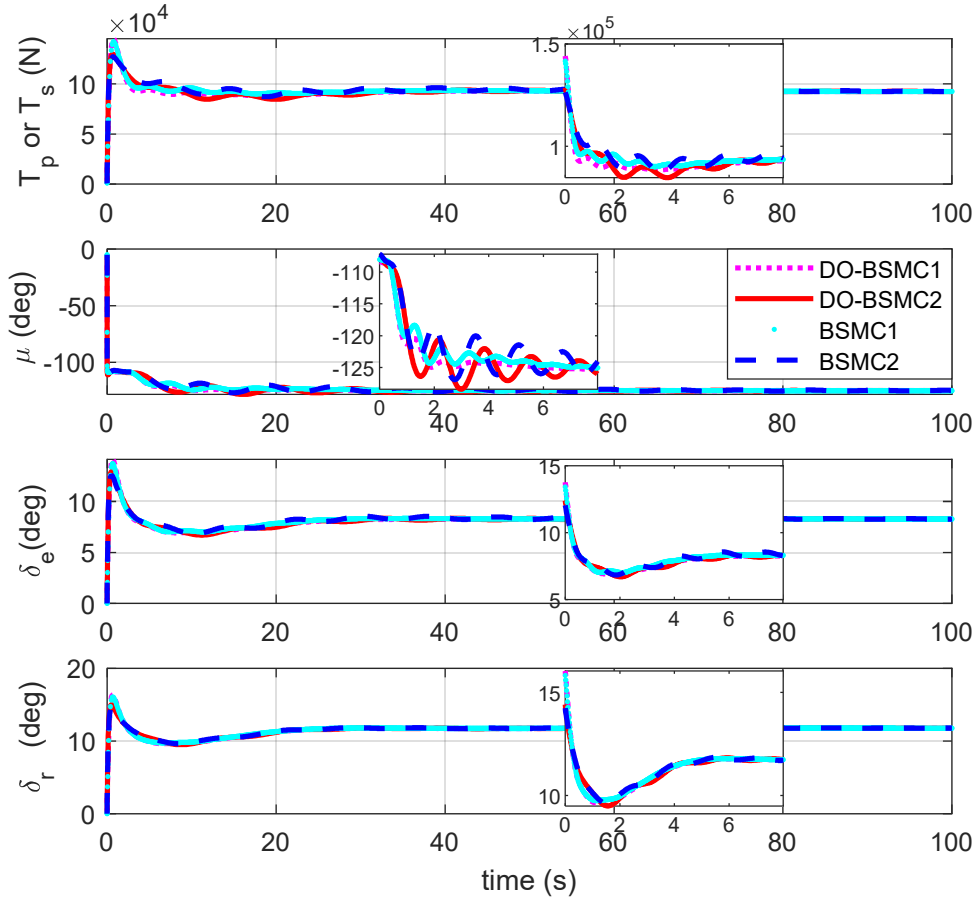

Fig. 16. Control inputs with model uncertainty and external disturbances.

Fig.16 shows the control inputs by using the DO-BSMC design are bigger than those by using the BSMC method due to disturbance observer based compensation, and the inputs of the BSMC2 approach are bigger than those by using the BSMC1 method.

Scenario III: Trajectory tracking control under parameter uncertainty and unknown disturbances and winds

In this scenario a 1- cosine wind is introduced to the system with above model uncertainties and constant disturbances. The shape of the wind is set as (Valente C. and Jones D., 2015)

$$V_w(x_d)=\begin{cases}\dfrac{U_{ds}}{2}\left(1-\cos\left(\dfrac{\pi x_d}{H}\right)\right), & for \quad 0\le x_d\le 2H\\ 0, & otherwise\end{cases} \tag{68}$$

where x_d is the distance penetrated into the wind, H is the distance parallel to the flight path of the airship for the wind to reach its peak velocity meeting $H = 0.5\,L_w$, L_w is wavelength of the wind, U_{ds} is the design wind velocity in equivalent air speed as follows

$$U_{ds} = U_{ref} F_w \left(\frac{H}{106.68} \right)^{1/6} \tag{69}$$

where U_{ref} is the reference gust velocity, F_w is the flight profile alleviation factor, $U_{ref} = 6.3$m/s at the altitude of 20000m, $F_w = 1$, and set V_{wx} *for* $0 \le x_d \le 2H$,V_{wy} *for* $2H \le x_d \le 4H$,V_{wz} *for* $4 \le x_d \le 6H$.

Choose a wind observer with the states $\begin{bmatrix} \hat{\boldsymbol{\xi}} \\ \hat{\boldsymbol{\upsilon}}_w \end{bmatrix}$, $\hat{\boldsymbol{\xi}}$ and $\hat{\boldsymbol{\upsilon}}_w$ denote estimation of $\boldsymbol{\xi}$ and $\boldsymbol{\upsilon}_w$, $\boldsymbol{\upsilon}_w$ denotes the wind speed vector, and design its dynamics as (Liu S. Q. andSang Y.J., 2020)

$$\begin{bmatrix} \dot{\hat{\boldsymbol{\xi}}} \\ \dot{\hat{\boldsymbol{\upsilon}}}_w \end{bmatrix} = \begin{bmatrix} \boldsymbol{R}(\boldsymbol{\eta})\upsilon_a \\ \boldsymbol{0} \end{bmatrix} + \begin{bmatrix} L_\xi & I_3 \\ L_w & \boldsymbol{0} \end{bmatrix} \begin{bmatrix} \boldsymbol{\xi} - \hat{\boldsymbol{\xi}} \\ \hat{\boldsymbol{\upsilon}}_w \end{bmatrix} \tag{70}$$

The estimation error can be obtained as

$$\dot{\boldsymbol{e}}_\upsilon = \begin{bmatrix} \boldsymbol{\xi} - \hat{\boldsymbol{\xi}} \\ \boldsymbol{\upsilon}_w - \hat{\boldsymbol{\upsilon}}_w \end{bmatrix} = \begin{bmatrix} -\boldsymbol{L}_\xi & \boldsymbol{I}_3 \\ -\boldsymbol{L}_w & \boldsymbol{0} \end{bmatrix} \boldsymbol{e}_\upsilon = \tilde{A}_e \boldsymbol{e}_\upsilon \tag{71}$$

where L_ξ , L_w are gain matrices subject to $\tilde{A}_e$ be Hurwitz,they are chosen as $L_\xi = diag(1,1,1)$, $L_w = diag(0.75, 0.75, 0.75)$.

By using the proposed BSMC and DO-BSMC design, the simulation results are shown in Figs 17-21.

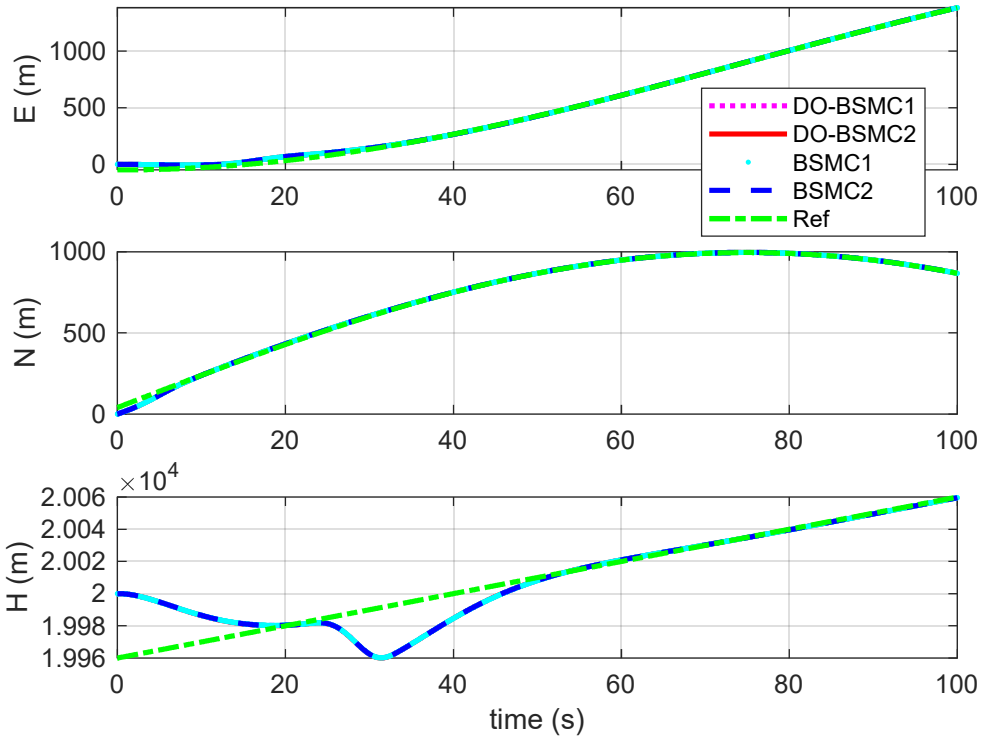

Fig. 17. Position tracking responses with disturbances, model uncertainties and winds

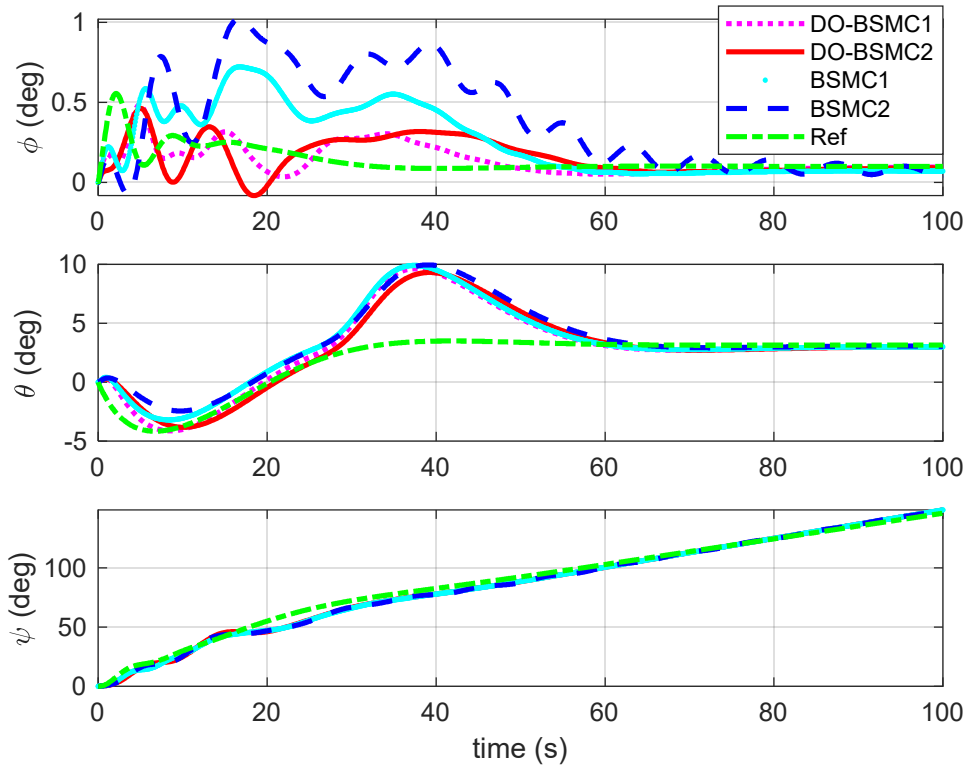

Fig. 18. Attitude tracking responses with disturbances, model uncertainties and winds

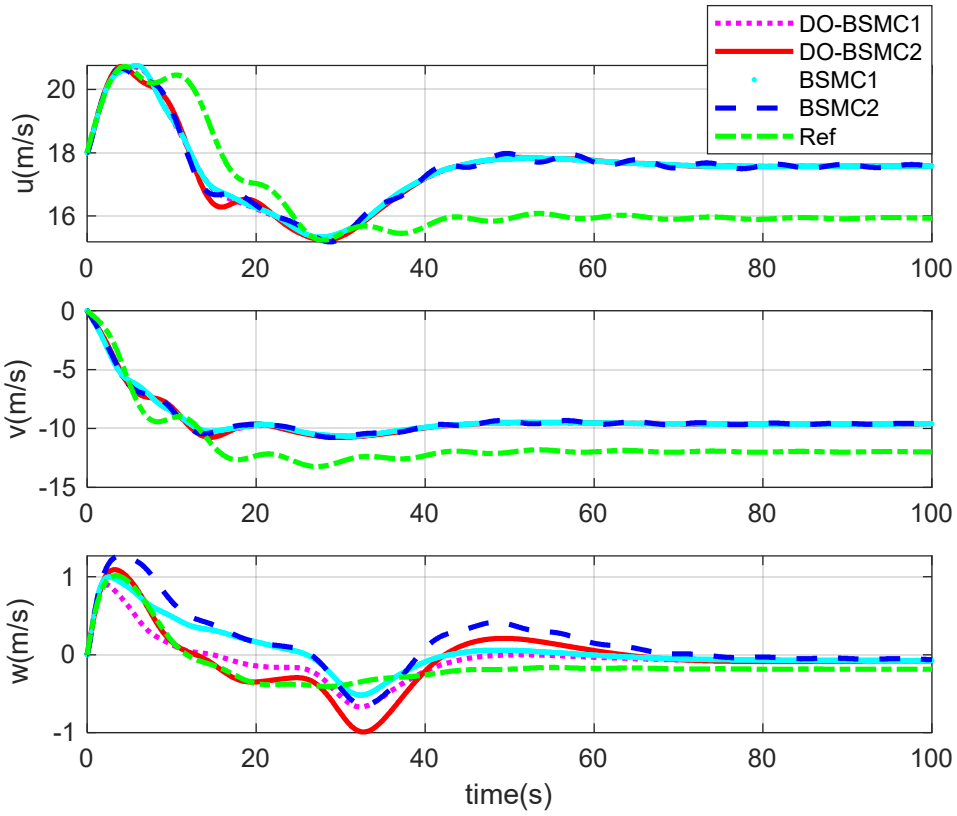

Fig. 19. Flight speed tracking responses with disturbances, model uncertainties and winds

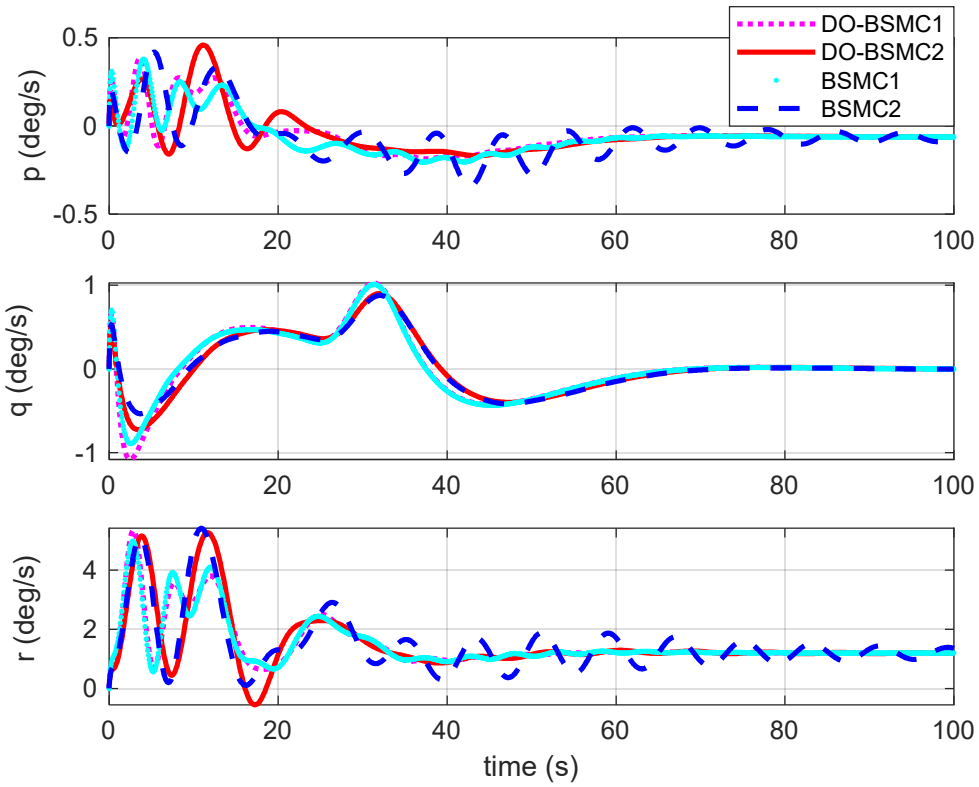

Fig. 20. Angular rate tracking responses with disturbances, model uncertainties and winds

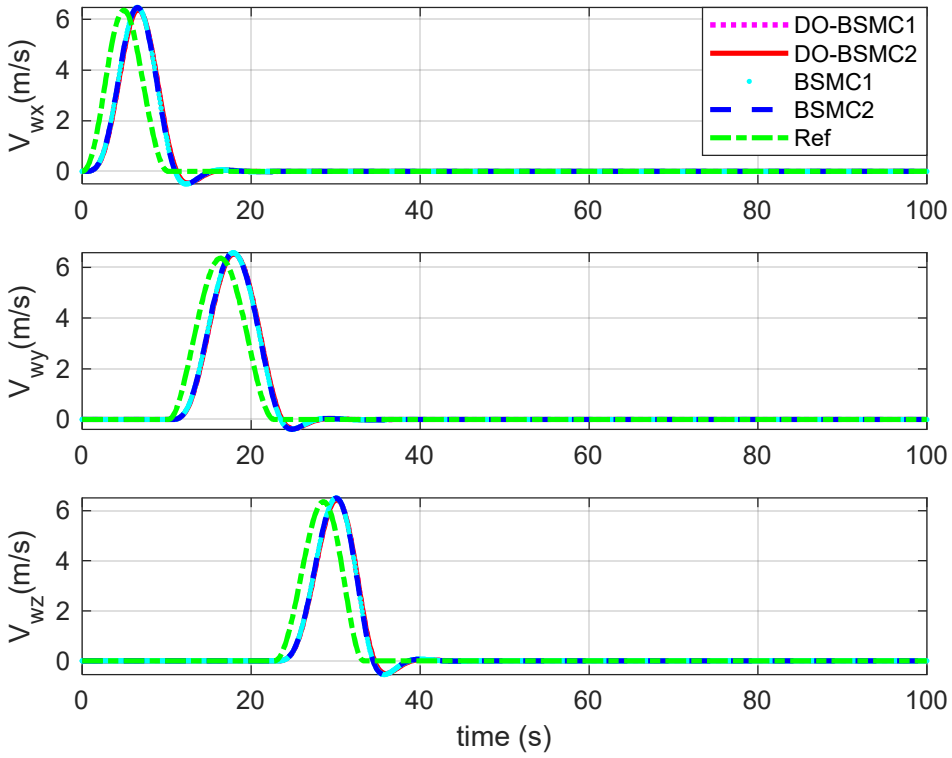

Fig. 21. Wind estimations under disturbances, model uncertainties and winds

From Fig.17-Fig.20, winds will affect the flight speed and position tracking responses, and generate some tracking errors, but the time of winds acting on the airship is bounded, so the tracking responses will approximate the desired values when the airship pass the wind field. Form Fig.21, it can be seen that the wind speeds have been precisely estimated by the proposed wind estimator. The estimation responses of winds have some time delay due to bandwidth limitation of the wind observer.

5. Conclusion

In this paper we propose two DO-BSMC control approaches for a stratospheric airship. Based on a full 6-DOF nonlinear model, the trajectory tracking controller is designed. The developed controller stabilizes the attitude and velocity of the airship via a backstepping sliding mode control method. Furthermore, a nonlinear disturbance observer is designed to reduce effect of the external unknown disturbances and model uncertainties for the trajectory tracking control. Stability analysis shows that the closed-loop trajectory

tracking error dynamics are globally asymptotically stable. Two cases of the unknown disturbances and model parameter uncertainties were simulated and show the proposed robustness. Compared with the BSMC controller, the DO-BSMC design achieve better trajectory tracking performances even though the airship is affected by parametric uncertainties and external bounded disturbances. Therefore, the effectiveness and availability of the DO-BSMC design are demonstrated.

Acknowledgements

This work has been funded by the National Natural Science Fund under the Grant 10577012. The work of Shiqian Liu was supported by the China Scholarship Council under the grant number 201806235014.

References

Azinheira J.R., Moutinho A., Paiva E.C. D., 2006. Airship hover stabilization using a backstepping control approach. *Journal of Guidance, Control, and Dynamics.* **29**(4), 903-914.

Azinheira J.R., Moutinho A., Paiva E.C.D., 2009. A backstepping controller for path-tracking of an underactuated autonomous airship. *International Journal of Robust and Nonlinear Control*. **19**(4), 418-441.

Adhikary N. and Mahanta C., 2013. Integral backstepping sliding mode control for underactuated systems: Swing–up and stabilization of the cart–pendulum system, *ISA Transactions*, 52(6), 870–880

Bolivar M. R., and Zinober A., 1994. Sliding mode control for uncertain linearizable nonlinear systems: A backstepping approach, *Proc. of the IEEE Work on Robust Control via Variable Structure and Lyapunov Techniques*, Benevento, Italy, Sep. 78-85

Bolivar M. R., and Zinober A., and Ramirez H. S., 1997. Dynamical adaptive sliding mode output tracking control of a class of nonlinear systems, *International Journal of Robust and Nonlinear Control*, **7(4)**, 387 – 405.

Chen B., 2017. Adaptive backstepping sliding mode tracking control for the stratospheric airship, *12th International Conference on Computer Science and Education* (ICCSE), (8), 202–207.

Chen, L, Edwards, C, Alwi, H. 2020. Sliding mode observers for a class of linear parameter varying systems. *International Journal of Robust and Nonlinear Control*, 30: 3134-3148.https://doi.org/10.1002/rnc.4951.

Chen W. H., Yang J., Guo L., and Li S.H., 2016. Disturbance-Observer-Based Control and Related Methods—an Overview, *IEEE Transaction on Industrial Electronics*, **63**(2), 1083–1095

Chen W. H., 2003. Nonlinear Disturbance Observer-Enhanced Dynamic Inversion Control of Missiles, *Journal of Guidance, Control, and Dynamics.* **26**(1):161-166

Chen W.H., Ballance D.J., Gawthrop P.J., and Reilly J. O, 2000. A nonlinear disturbance observer for robotic manipulators. IEEE Transations on Industrial Electionics, 47(4), 932–938.

Edwards C. and Spurgeon S., 1998. Sliding Mode Control: Theory and Applications. CRC Press, ch. 1.

Fossen T.I.,1994. *Guidance and Control of Ocean Vehicles,* Appendix C. John Wiley & Sons LTD, 411-412.

Fossen T.I., Strand J. P., 1999. Tutorial on nonlinear backstepping: application to ship control, *Modeling, Identification and Control*, **20** (2), 83-134

Guo L., Chen W. H., 2005. Disturbance attenuation and rejection for systems with nonlinearity via DOBC approach, *International Journal of Robust and Nonlinear Control*. 15:109–125

Gomes S. B. V., An investigation into the flight dynamics of airships with application to the YEZ-2A. Dissertation for the Doctoral Degree. Cranfield University, 1990.

Hu J. S., Huang J. Z., Gao Z. X., Gu H.B., 2018. Position tracking control of a helicopter in ground effect using nonlinear disturbance observer-based incremental backstepping approach, *Aerospace Science and Technology*. (81), 167–178

Liesk T., Nahon M., Boulet B., 2013. Design and experimental validation of a nonlinear low-level controller for an unmanned fin-less airship. *IEEE Transactions on Control Systems Technology*. **21**(1), 149-16

Liu S. Q., Sang Y. J., 2018. Underactuated stratospheric airship trajectory control using an adaptive integral backstepping approach, *Journal of Aircraft*, **55** (6), 2357-2371

Lou W. J., Zhu M. , Guo X., and Liang H.Q., 2019. Command filtered sliding mode trajectory tracking control for unmanned airships based on RBFNN approximation, *Advances in Space Research*, 63(3), 1111-1121

Liu S. Q., Sang Y. J., Whidborne J. F., 2020. Adaptive sliding-mode-backstepping trajectory tracking control of underactuated airships, *Aerospace Science and Technology*, (97), 1-13.

Li S.H., Yang J., Chen W. H., , Chen X.S., 2014. *Disturbance Observer-Based Control- Methods and Applications*, CRC press, ch14, 233-300

Moutinho A. and Azinheira J.R., 2006. A Gain-scheduling approach for airship path-tracking , *Informatics in Control Automation and Robotics*. Selected Papers from the International Conference on Informatics in Control Automation and Robotics, Springer Press, (15), 263-275

Moutinho A., Azinheira J.R., 2004., Path control of an autonomous airship using dynamic inversion, IFAC Proceedings, (37), 633-638

Moutinho A., Azinheira J.R., Paiva E.C. D., Bueno S.S., 2016. Airship robust path tracking: A tutorial on airship modeling and gain scheduling control design. *Control Engineering Practice*. (50), 22-36

Mueller J.B., Paluszek M.A., Zhao Y., 2004. Development of an aerodynamic model and control law design for a high altitude airship, in: *AIAA 3rd Workshop and Exhibit of "Unmanned Unlimited" Technical Conference,* Chicago, Illinois, USA , 1-17.

Parsa A., Monfared S. B., and Kalhor A., 2018. Backstepping control based on sliding mode for station-keeping of stratospheric airship, *6th RSI International Conference on Robotics and Mechatronics* (IcRoM), 554–559.

Slotine J.-J. E. and Li W., 1991. Applied Nonlinear Control. Englewood Cliffs (N.J.): Prentice Hall, ch. 6.

Valle R. C., Menegaldo L.L., Simões A. M., 2015. Smoothly gain-scheduled control of a tri-turbofan airship. *Journal of Guidance, Control, and Dynamics.* **38**(1), 1-16.

Vieira H. S., 2019. Projeto unificado de controladores não lineares para umdirigível robótico de propulsão elétrica. Ph.D. dissertation, Universidade Estadual de Campinas.

Valente C., Jones D., GaitondeA., Cooper, J. E., and Lemmens, Y., 2015. Openfsi interface for strongly coupled steady and unsteady aeroelasticity. *International Forum on Aeroelasticity and Structural Dynamics* (IFASD). IFASD 2015, pp. 591-606.

Yang N., Yan Y., 2016. Neural network approximation-based nonsingular sliding mode control for trajectory tracking of robotic airships, *Aerospace Science and Technology*. (54), 192–197

Zheng Z.W., Sun L., 2018. Adaptive sliding mode trajectory tracking control of robotic airships with parametric uncertainty and wind disturbance, *Journal of the Franklin Institute*, (355) , 106–122

Yang Y.N., 2018. A time-specified nonsingular terminal sliding mode control approach for trajectory tracking of robotic airships. *Nonlinear Dynamics*. (92), 1359–1367.

2020-11-16

Backstepping sliding-mode control of stratospheric airships using disturbance-observer

Liu, Shi Qian

Elsevier

Liu SQ, Whidborne JF, He L. (2021) Backstepping sliding-mode control of stratospheric airships using disturbance-observer. Advances in Space Research, Volume 67, Issue 3, February 2021, pp. 1174-1187

https://doi.org/10.1016/j.asr.2020.10.047